DNA replication stress and the subsequent activation of DNA damage checkpoint (10, 11). The checkpoint functions as an inducible barrier against genomic instability and tumor development (12, 13). The probable prelymphoma cells may exhibit the activation of DNA damage checkpoint, or they may show difference in oncogenic signals because lymphomas/leukemias are distinct in origin from carcinomas. Indeed, some disagreement has been reported in the study of T cell lymphomas developed in *PTEN*-deficient mice (14). In this study, we have characterized the probable prelymphoma cells showing clonal growth and changes in signaling, including DNA damage checkpoint.

METHODS AND MATERIALS

Mice and induction of atrophic thymus and lymphoma development

BALB/cAJcl mice (purchased from CLEA Japan, Tokyo, Japan) were mated with MSM mice (provided from Dr. Shiroishi, NIG at Mishima), and their male and female progeny were subjected to whole-body γ-irradiation of 2.5 Gy (^{137}Cs) four times at a weekly interval, starting at the age of 4 weeks. Thymus was isolated at 40 days and 80 days after the start of irradiation. Isolation of thymic lymphomas and bone marrow cell transfer were carried out as described previously (15, 16). Mice used in this study were maintained under specific pathogen-free conditions in the animal colony of Niigata University. All animal experiments comply with the guidelines of the animal ethics committee for animal experimentation of the University.

Flow cytometry

Flow cytometric analysis and 5-bromo-2-deoxyuridine (BrdU) incorporation experiments were performed as previously described (17). The monoclonal antibodies used were anti-CD4-FITC or -APC (RM4-5), anti-CD8-APC (53-6.7), purchased from eBioscience (San Diego, CA). Anti-Nrp-1 (sc-5541; Santa Cruz Biotechnology, Santa Cruz, CA) was detected with anti-rabbit IgG-Alexa Fluor 488 (A11008; Molecular Probes, Eugene, OR). Dead cells and debris were excluded from the analysis by appropriate gating of FSC and SSC. Cells were analyzed by a FACScan (Becton-Dickinson, Franklin Lakes, NJ) flow cytometer, and data were analyzed using FlowJo software (Tree-Star, Ashland, OR).

DNA isolation and PCR analysis

Deoxyribonucleic acid was isolated from brain, thymocytes, and thymic lymphomas using the DNeasy Tissue Kit (Qiagen, Valencia, CA). To determine D-J rearrangement patterns in the *TCRβ* locus, polymerase chain reaction (PCR) was performed as described previously (16). For allelic loss analysis at *Bcl11b*, *D12Mit53* and *D12Mit279* markers were used for PCR as described previously (15). The PCR products were analyzed by 8% polyacrylamide gel electrophoresis, and band intensities were quantitated with a Molecular Imager FX (Bio-Rad Laboratories, Hercules, CA) after ethidium bromide staining to determine the allele ratio of BALB/c and MSM alleles.

Antibodies for Western blotting

Sample preparation and Western blotting were performed as described previously (18). Antibodies used are listed below. Anti-H2AX (ab11175) and anti-Chk2 (pT68) (ab38461) were purchased from Abcam (Cambridge, MA). Anti-p27 Kip1 (#2552), anti-Chk2 (#2662), anti-p53 (pSer15) (#9284), anti-Akt (#9272), and anti-Akt (pSer473) (#4058) were purchased from Cell Signaling Technology (Danvers, MA). Anti-cMyc (sc-42), anti–proliferating cell nuclear antigen (PCNA) (sc-7907), anti-actin (sc-1615), anti-p53 (sc-1312), anti-Chk1 (sc7898), and horseradish peroxidase (HRP)-anti-goat IgG (sc-2020) were purchased from Santa Cruz Biotechnology. Anti-cyclin D1 (K0062-3) was purchased from MBL (Nagoya, Japan). Anti-Chk1(pS317) (AF473) was purchased from R&D Systems (Minneapolis, MN). Horseradish peroxidase-anti-rabbit IgG (NA934 V) and HRP-anti-mouse IgG (NA931VS) were purchased from Amersham. Anti-γH2AX (Ser139) (#07-164) was purchased from Upstate (Temecula, CA).

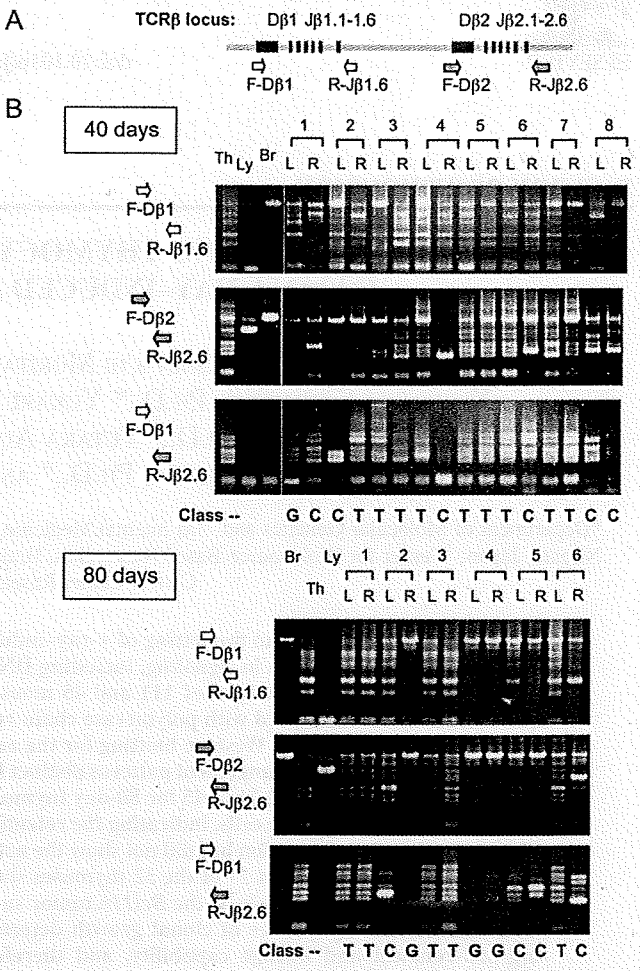

Fig. 1. Clonal growth of thymocytes in atrophic thymuses at 40 days and 80 days after γ-irradiation. (A) Diagram showing part of the *TCRβ* locus and the relative location of polymerase chain reaction (PCR) primers used. (B) Gel electrophoresis of PCR products with three different sets of primers: F-Dβ1 and R-Jβ1.6 (top), F-Dβ2 and to-Jβ2.6 (middle), and F-Dβ1 and R-Jβ2.6 (bottom). Th = thymus; Ly = lymphomas; Br = barain DNA; L and R = left and right thymic lobe; T = T type thymus; C = C type thymus; G = G type thymus.

RESULTS

Clonal expansion of thymocytes in γ-ray–induced atrophic thymus

Clonality of thymocytes was examined in left and right lobes separately of atrophic thymuses at 40 and 80 days after

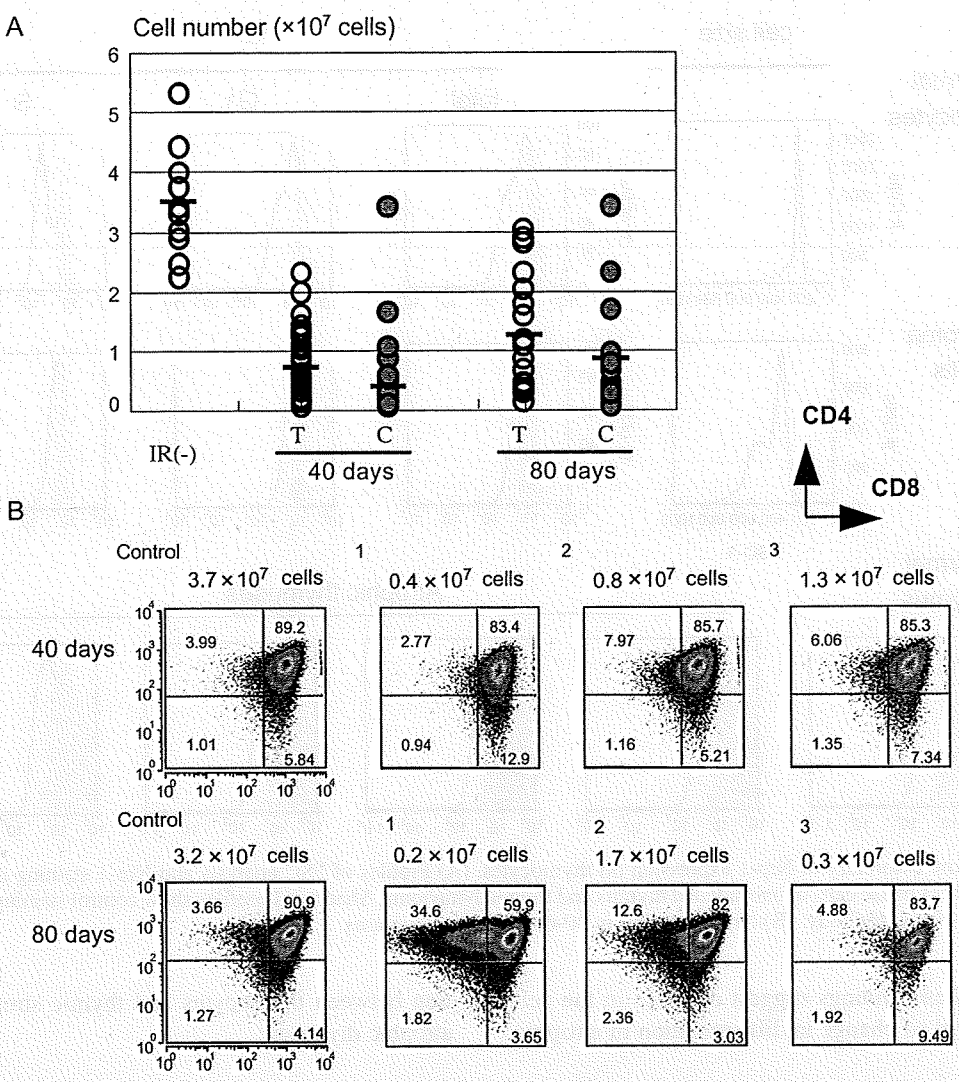

Fig. 2. Reduced cellularity and minimal changes of thymocyte differentiation in atrophic thymuses. (A) Cell numbers of thymocytes in unirradiated thymus and the atrophic thymuses at 40 days and 80 days after irradiation, which were divided into the T type (T) and C type (C) thymus. Bars indicate averages. (B) Flow cytometric analysis of thymocytes from C type thymuses using CD4 and CD8 cell-surface markers. Numbers in quadrants indicate percentage of cells.

γ-irradiation (hereafter these thymic lobes are designated as 40-day and 80-day thymuses, respectively). The earliest time of appearance of fully malignant thymic lymphomas is approximately 100 days after irradiation, and 60% of mice develop lymphomas at 300 days after (5, 16). Clonality was determined in 111 samples of 40-day thymuses and 45 samples of 80-day thymuses by assaying specific V(D)J rearrangements with three primer sets designed for the *TCRβ* locus (16). Figure 1 shows examples, and Supplementary Figs. E1A and B display others. Unirradiated thymus (lane Th) gave six different bands corresponding to possible recombination sites between D and J regions by Dβ1-Jβ1, Dβ2-Jβ2, and Dβ1-Jβ2 probe sets and one band for germline DNA by the former two probe sets. On the other hand, thymic lymphoma DNA (Ly) gave one band only by the Dβ2-Jβ2 probe set used, and brain DNA (Br) gave the germline DNA band by Dβ1-Jβ1 and Dβ2-Jβ2 probe sets. Half (52 of 111) of the 40-day thymuses showed rearrangement patterns identical or similar to that of the control thymus, classified as T type thymus. Most others (43) exhibited only few bands or limited numbers of bands. This group of the thymuses indicated the existence of clonally expanded thymocytes (C type thymus). Several thymuses were classified as C/T type thymus. The fourth group comprised 12 thymuses that exhibited mainly one germline band, probably consisting of immature thymocytes and/or cells other than thymocytes. This study excluded analysis of the G type thymus because of its low incidence. Of the 80-day thymuses, 22 thymuses belonged to T type thymus, and 20 were C type thymus.

Figure 2A shows the thymocyte numbers of 40-day and 80-day thymuses. The average decreased by approximately one seventh in 40-day thymuses, and the decrease tended to be more in C type thymus than in T type thymus. The tendency of decrease was continued in 80-day thymuses. Flow cytometry using CD4 and CD8 cell-surface markers revealed that most thymocytes were DP cells, as normal thymocytes

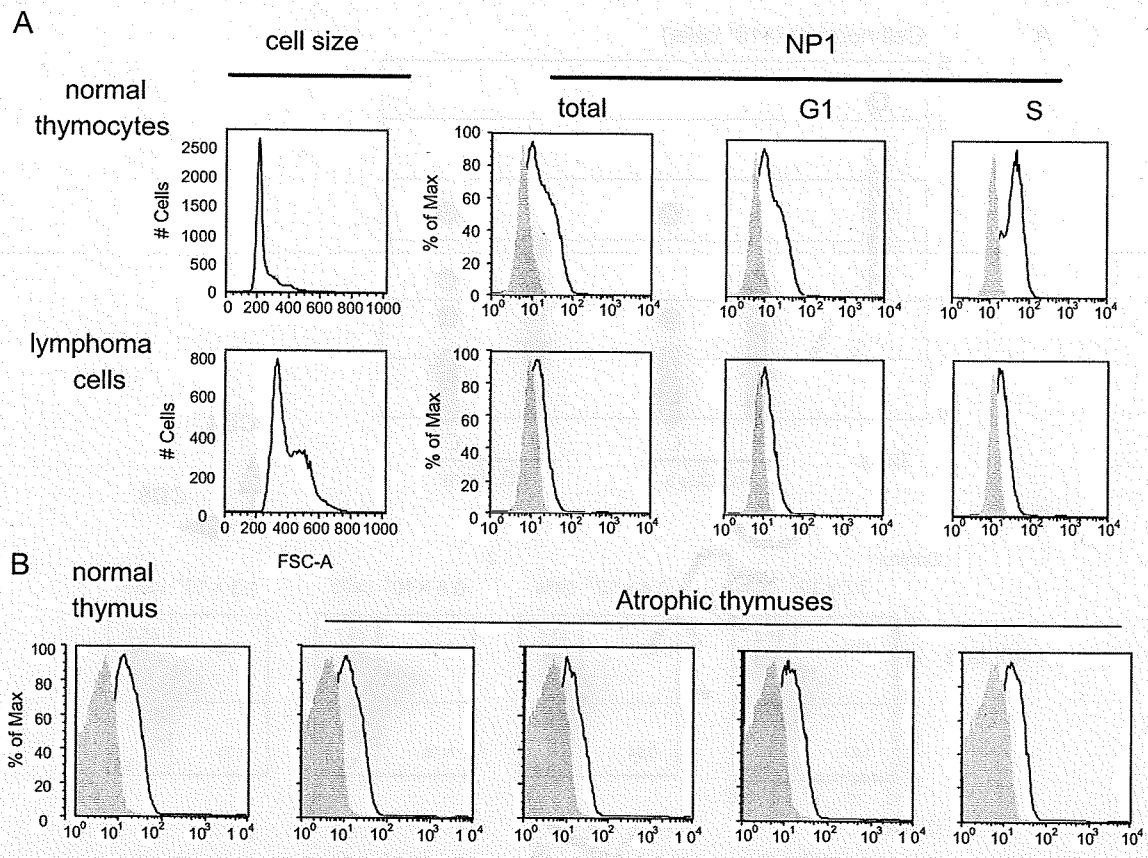

Fig. 3. Flow cytometry of Nrp-1 expression on thymocytes. (A) Profiles of FSC analysis and Nrp-1 staining in total, S phase, and G1 phase cells of unirradiated thymus and thymic lymphoma. Shadowed profiles show control staining without using anti-Nrp-1 antibody. (B) Nrp-1 staining in 40-day atrophic thymuses. Q7

were (Fig. 2B). These findings suggest decrease in the cell number and no marked change in differentiation in atrophic thymus.

Bone marrow cell transfer to irradiated mice 1 week after the last irradiation suppresses the development of thymic lymphomas (1). To confirm this, we examined eight thymic lobes at 60 days after bone marrow cell transfer. As predicted, the cell number was restored to the normal level (3.1×10^7 cells on average), and no C type thymuses were found (not shown).

Nrp-1 expression in atrophic thymuses

Nrp-1 proteins are expressed on the cell surface of both thymocytes and thymic epithelial cells and play a key role in heterocellular adhesions (19, 20). We examined Nrp-1 on thymocytes in normal thymus, thymic lymphomas, and 16 40-day atrophic thymuses using flow cytometry. Levels of Nrp-1 expression on normal thymocytes varied in different phases of the cell cycle, higher in S cells than G1 cells (Fig. 3A). On the other hand, levels on lymphoma cells were lower than those on normal thymocytes and did not much differ between S and G1 cells. Figure 3B shows examples of 40-day atrophic thymuses. Most of them exhibited expression levels similar to that of the control. Neither was any marked difference seen between T type and C type thymus (not shown). These results suggest persistence of the interaction between thymocytes and thymic stroma cells even in atrophic thymuses.

Allelic loss at Bcl11b in C type and T type thymuses

Clonal expansion of thymocytes may result from genetic changes. Hence, we examined allelic loss at *Bcl11b* tumor suppressor gene locus, which was detected at a high frequency in thymic lymphomas (15). *Bcl11b* encodes zinc finger transcription factors involved in the development of $\alpha\beta$ T cells (17). Mice used for this experiment were F_1 hybrids between BALB/c and MSM strains, and hence allelic differences were easily detectable with PCR. Figure 4A shows examples of 40-day thymuses including D-J rearrangement patterns (see Fig. E2A for others). We determined the BALB/c and MSM band ratio in a total of 95 40-day atrophic thymuses and compared the ratios between each atrophic thymus and normal F_1 mouse thymus. When the ratio was >2 or <.50, the thymus was judged as allelic loss-positive (Fig. 4B). The loss was detected in not only C type but also T type thymuses. Nineteen (44%) of the 43 C type thymuses and 17 (33%) of the 52 T type thymuses were allelic loss-positive (Fig. 4C). The high frequency observed in T type thymuses was unexpected. This suggests that clonal expansion of this type proceeds in T type DP thymocytes before β-selection.

Analysis of 80-day thymuses (Fig. E2B) showed that 10 (50%) of the 20 C type thymuses but only 1 (5%) of the 22

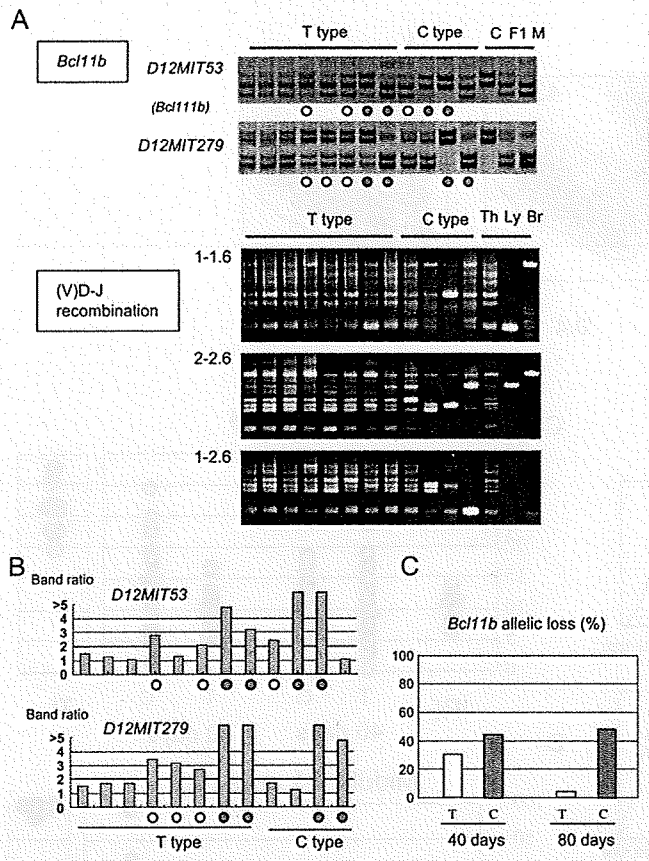

Fig. 4. Allelic losses at the *Bcl11b* locus. (A) Top two panels show polyacrylamide gel electrophoresis for polymerase chain reaction products of *D12Mit53* and *D12Mit279* primer pairs. Chromosomal location of *D12Mit53*, *Bcl11b*, and *D12Mit279* is 108.69 Mb, 109.15–24 Mb, and 109.69 Mb from the centromere, respectively. Bottom three panels show D-J rearrangement patterns, which identifies T type or C type thymus. Closed circles show allelic loss and open circles exhibit allelic imbalance. Thymuses that exhibited allelic loss in at least one of the two loci were decided as allelic loss positive, and this decision was based on three independent polymerase chain reaction experiments. Th = thymus; Ly = lymphomas. (B) Band ratios of BALB/c vs MSM or MSM vs BALB/c are shown relative to that of normal F_1 mouse thymus. Allelic losses are marked by filled circles and allelic imbalances by open circles. (C) Percentage of allelic loss in 40-day and 80-day thymuses that were divided into T type and C type thymus.

T type thymuses exhibited allelic loss. One reason for this rareness relative to 40-day T type thymuses ($p < 0.001$) might be that those T type thymocytes undergo normal differentiation process and hence are not retained within the thymus.

Characteristics of clonally expanded thymocytes

To characterize clonally expanded thymocytes, we examined the cell cycle of the 95 40-day and 42 80-day thymocytes that were isolated from mice 1 h after injection of BrdU (Fig. 5A and B, Fig. E3). We defined the gated region on the FSC vs. SSC dot plot to exclude debris and dead cells. The percentage of the gated region markedly decreased, suggesting enhanced apoptosis. Figure 5B shows BrdU incorporation levels at the vertical axis and DNA contents at the horizontal axis. The DNA content of G1 cells did not differ among unirradiated, irradiated thymocytes, and lymphoma cells, which is consistent with the finding that even thymic lymphoma cells sustain diploidy (21). Figure 5C summarizes the percentage of S phase cells in T type and C type thymuses. Of the 40-day thymuses, no marked difference was found between T and C type thymuses. However, significant increase in the percentage was seen in C type thymus relative to T type thymus in the 80-day thymuses ($p = 0.0034$). Of note is that the high percentage of S cells is a hallmark of thymic lymphomas.

The size of G1 phase cells was measured with flow cytometry (Fig. 5B), because it represents the level of cell cycle progression and metabolic activity. The FSC values of G1 cells depicted a sharp peak in normal thymus, indicating a rather homogeneous cell-size population. The values were much smaller than those of S cells showing a broad peak, as predicted. The FSC analysis of 40-day and 80-day thymuses tended to show the values larger than normal thymus. The cell size of G1 cells in some atrophic thymuses exhibited a broad peak, indicating that those thymuses contained a fraction of larger-sized G1 cells more than normal thymuses did. We designated the cells in this fraction as middle-sized G1 cells because their size was between that of normal G1 and S phase cells. The middle-sized cells may be related to premalignancy because the cell-size enlargement was another characteristic of thymic lymphomas. The middle-sized G1 thymocytes are probably cells that are growing and progressing toward S phase but pausing at the late G1 stage.

Figure 5D summarizes the percentage of middle-sized G1 cells within the thymus. The percentage was determined in each thymus by the criterion whereby the percentage in normal thymus was set to approximately 5% in FSC analysis. The percentage showed a significant difference between T and C type thymuses in 40-day thymuses ($p = 0.014$), and the difference was more prominent in 80-day thymuses ($p = 0.0002$). Half of the 80-day C type thymuses exhibited the percentage more than 40%, whereas only 4 did so in the 21 T type thymuses. Notably, all thymic lymphomas consisted of middle-sized cells, suggesting that the C type middle-sized thymocytes are closer to lymphoma cells. Comparison between 40-day and 80-day thymuses suggests a process of irradiated thymuses toward thymic lymphoma in the order of T type thymus, C type thymus with a low percentage of middle-G1 cells, and C type thymus with a high percentage of middle-G1 cells.

Figure 5E summarizes the percentage of middle-sized G1 cells in *Bcl11b* allelic loss-negative and -positive thymuses. The two groups of 40-day thymuses showed difference in the percentage ($p = 0.041$). The 80-day thymocytes also showed a difference between the two ($p = 0.017$). This suggests the contribution of *Bcl11b*-allelic loss to cell cycle progression. On the other hand, no significant difference in the percentage of S cells was observed between the two groups (not shown).

No marked change in DNA damage checkpoint response

Deoxyribonucleic acid damage checkpoints are activated in premalignant cells and thought to act as barriers against

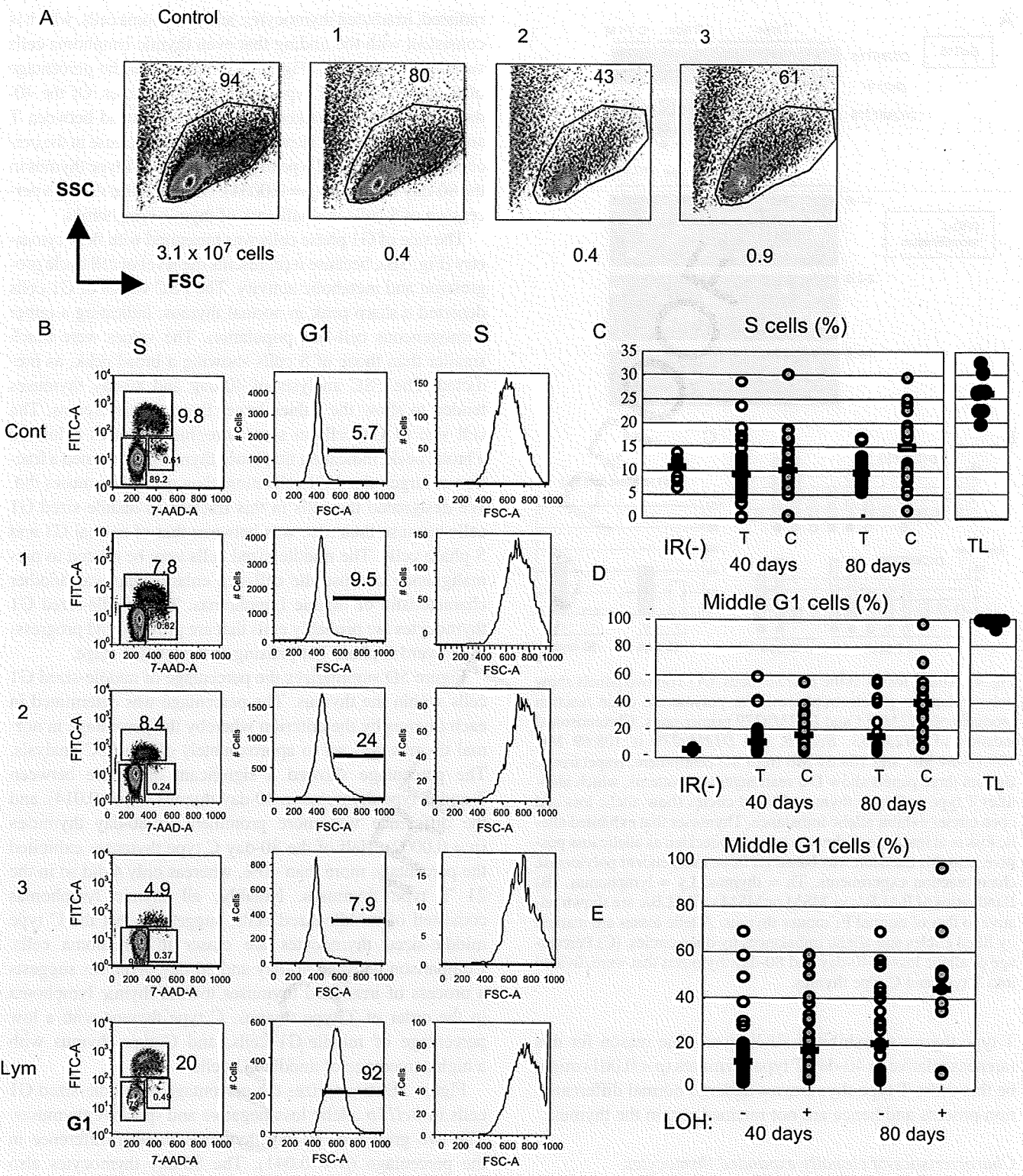

Fig. 5. Hindrance in cell cycle. (A) Flow cytometry of thymocytes in control and irradiated atrophic thymuses. The indicated area is the gated region to exclude dead cells and debris. (B) Flow cytometry of cell cycle and cell size. Left: Vertical axis shows 5-bromo-2-deoxyuridine incorporation levels, and the horizontal axis displays 7-AAD staining for DNA contents. Middle, Right: Vertical axis shows cell number, and the horizontal axis displays FSC values reflecting the cell size in G1 and S phase thymocytes. The bar in G1 cell analysis shows a fraction of thymocytes of the indicated larger cell sizes, and the number above the bar indicates the percentage of those thymocytes. (C) Percentages of S-phase thymocytes in unirradiated thymus and the atrophic thymuses at 40 days and 80 days after irradiation, which were divided into T type and C type thymus. (D) Percentages of middle-sized G1 cells in the different groups of thymuses as indicated above. (E) Percentages of middle-sized G1 cells in unirradiated thymus and the atrophic thymuses at 40 days and 80 days after irradiation (IR), which were divided into the *Bcl11b* allelic loss-negative and -positive thymus.

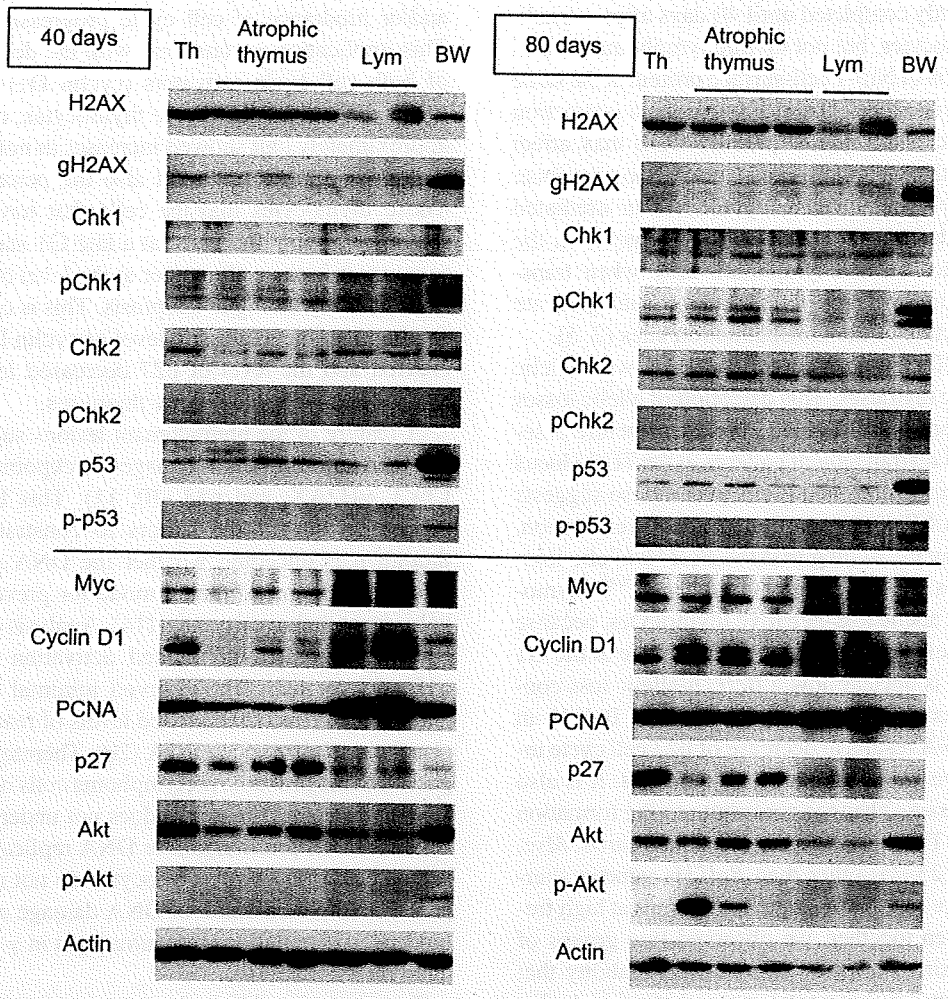

Fig. 6. No marked activation of DNA damage checkpoint genes in C type atrophic thymuses at 40 days and 80 days after irradiation. Western blot analysis includes unirradiated thymus (Th), thymic lymphomas (Lym), and BW5147 mouse T cell lymphoma cell line (BW) for comparison. Antibody used is shown left of each panel. Some BW5147 cell samples were isolated after γ-irradiation. The cell number of the three 40-day thymuses was 4.0, 8.0, and 6.0 × 10^6, respectively, and that of the three 80-day thymuses was 2.4, 2.5, and 1.8 × 10^7, respectively.

cancer development (10–13). To examine the checkpoint status in C type atrophic thymuses, we performed Western blot analysis for proteins involved in the checkpoint responses H2AX, Chk1, Chk2, and p53 (Fig. 6). For comparison, thymic lymphomas and BW5147 mouse T cell lymphoma cell line were analyzed. No difference in their activation was observed between normal thymus and either 40-day or 80-day atrophic thymuses. Another nine samples of 40-day thymuses also showed similar results (not shown). Only p53 amount showed minimal increases in some of the atrophic thymuses. These results indicated no activation of DNA damage checkpoints in C type atrophic thymuses.

Figure 6 includes analysis of Myc, cyclin D1, PCNA, and p27, which are related to cell cycle progression, and Akt, which is related to cell size (22). Expression of cyclin D1 and PCNA was decreased in the 40-day C type atrophic thymuses, whereas expression of p27 cdk-inhibitor also tended to decrease. No activation was noted in Akt. Of the 80-day C type atrophic thymuses, levels of cyclin D1 and PCNA expression increased relative to the 40-day thymuses. On the other hand, the decrease of p27 was more marked, and phosphorylation of Akt was noted in some of the thymuses. These results indicated changes in signaling pathways of cell cycle and cell size in some of the 80-day C type atrophic thymuses.

DISCUSSION

Prelymphoma is assumed to exist in the γ-ray–induced atrophic thymus (1, 2). In this study, we characterized thymocytes in the atrophic thymus and changes in signaling pathways in those thymocytes. Approximately 40% of 40-day thymocytes (harvested 40 days after irradiation) at an early stage during lymphomagenesis showed limited D-J rearrangement patterns at the *TCRβ* locus, indicating clonal expansion of a few parental thymocytes having passed β-selection. Despite their clonal expansion, the C type thymocytes mainly consisted of $CD4^+CD8^+$ DP cells, suggesting retention of the differentiation capability. The percentage of C type thymus in 80-day thymuses was similar to that in 40-day thymuses. This suggests that the generation of C

type thymus is mostly completed until 40 days after γ-irradiation. C type thymocytes, but not thymic lymphomas, maintained the expression of Nrp-1 cell-surface protein at the same level of normal thymocytes. This maintenance in interaction between thymocytes and thymic epithelial cells may affect the cellular fate of those thymocytes. It might also contribute to lymphoma development when thymocytes in irradiated mice are transplanted (1). This speculation is based on the fact that thymocytes formed lymphoma only when transplanted in the thymus, whereas lymphomas could generate lymphoma irrespective of the transplantation sites (2, 5).

Among the 95 40-day atrophic thymuses, 17 were allelic loss-positive T type thymuses. This detection of allelic losses reflects clonal expansion of a given thymocyte before β-selection because D-J rearrangement patterns at the *TCRβ* locus were the same as that of normal thymocytes. It also suggests that the allelic loss of *Bcl11b* contributes to clonal expansion. This is supported by the finding that the *Bcl11b* allelic loss-positive thymocytes were enriched in middle-G1^{high} thymocytes more than the allelic loss-negative thymocytes, because this suggests the elevated stimulation of cell cycle at the G1 phase. However, it is unclear how a *Bcl11b*-allelic loss contributes to clonal expansion. Downregulation of Bcl11b in Jurkat cells by siRNA results in decrease of p27 cell cycle inhibitor (18), and this may support that hypothesis. It is also not known what genetic changes contribute to the formation of C type thymus. The candidate may include *Ikaros*, *Myc*, *Notch1*, and *Pten* (23–25) other than *Bcl11b*, genetic alterations of which were found in thymic lymphomas at high frequencies (15). Taken together, we observed two groups of thymocytes possessing intrinsic self-renewal capability that occurred at different developmental stages before and after β-selection. Both the *Bcl11b* allelic loss-positive T type and the C type thymocytes retain the capability to differentiate. Because the T type thymocytes were similar to normal thymocytes in cell size, they might be a precursor of C type thymocytes, but their relationship remains to be clarified.

The percentage of middle-sized G1 cells was increased in C type thymuses more than in T type thymuses. Those thymocytes may be cells that tend to pause at a late G1 stage before the cell-grown stage entering into S phase. The increase in the fraction of such middle G1 cells may reflect stimulation and/or hindrance of cell cycle progression of thymocytes. This implication is consistent with the decreased expression of both cell cycle activators (cyclin D1) and the inhibitor (p27). Of the 80-day C type thymocytes, on the other hand, approximately half showed increases in not only the percentage of middle G1 cells but also the percentage of S cells. Those thymocytes may be cells that have overcome hindrance(s) giving the pause at a late G1 stage but still failed to increase in the cell number at the level of thymic lymphomas, possibly owing to apoptosis. This is consistent with the finding that the expression level of cyclin D1 and PCNA increased and the level of p27 decreased in the 80-day thymuses relative to the 40-day thymuses.

A feature of the premalignant lesions such as dysplasia is the activation of DNA damage checkpoints, such as Chk1, Chk2, γH2AX, and p53 (10, 11). This DNA damage response is one of the barriers to constrain tumorigenesis, though it is uncertain whether the DNA damage response represents the predominant mode for preventing cancer development at the early stage (14). Analysis of the C type thymocytes revealed no marked activation in Chk1, Chk2, γH2AX, or p53. The observed minimal increases of p53 might be ascribed to increased levels of reactive oxygen species that stabilize p53 mRNA (26). Therefore, the result suggests that the probable prelymphoma cells in atrophic thymus are an exceptional case that does not undergo aberrant stimulation of cell proliferation or DNA replication stress. If this is the case, the C type thymocytes do not undergo selective pressure for inactivation of DNA damage checkpoint genes. Indeed, *p53* mutations were infrequent in γ-ray–induced thymic lymphomas (16).

To summarize, this study characterizes clonally expanding thymocytes in γ-ray–induced atrophic thymus that occurs at two distinct developmental stages before and after β-selection. The thymocytes resemble CML in possessing self-renewal and lineage capacity. Therefore, they can be a candidate of the lymphoma-initiating cells, and the importance of leukemia/lymphoma-initiating cells is pointed out in relapsed acute lymphoblastic leukemia in humans (9). The mouse lymphoma model, including *Bcl11b*-KO and *Bcl11b*-floxed mice, will provide new insights into leukemia/lymphoma-initiating cells, a target of radiation and chemical therapy.

REFERENCES

1. Muto M, Kubo E, Sado T. Development of prelymphoma cells committed to thymic lymphomas during radiation-induced thymic lymphomagenesis in B10 mice. *Cancer Res* 1987;47:3469–3472.
2. Sado T, Kamisaku H, Kubo E. Bone marrow-thymus interactions during thymic lymphomagenesis induced by fractionated radiation exposure in B10 mice: Analysis using bone marrow transplantation between Thy 1 congenic mice. *J Radiat Res* 1991;32:168–180.
3. Penit C. In vivo thymocyte maturation. BUdR labeling of cycling thymocytes and phenotypic analysis of their progeny support the single lineage model. *J Immunol* 1986;137:2115–2121.
4. Gray DH, Ueno T, Chidgey AP. Controlling the thymic microenvironment. *Curr Opin Imnunol* 2005;17:137–143.
5. Kominami R, Niwa O. Radiation carcinogenesis in mouse thymic lymphomas. *Cancer Sci* 2006;97:575–581.
6. Calabretta B, Perrotti D. The biology of CML blast crisis. *Blood* 2004;103:4010–4022.
7. Mullighan CG, Miller CB, Radtke I, *et al.* BCR-ABL1 lymphoblastic leukaemia is characterized by the deletion of Ikaros. *Nature* 2008;453:110–114.
8. Clarke MF, Dick JE, Dirks PB, *et al.* Cancer stem cells—perspectives on current status and future directions: AACR Workshop on cancer stem cells. *Cancer Res* 2006;66:9339–9344.
9. Mullighan CG, Phillips LA, Su X, *et al.* Genomic analysis of the clonal origins of relapsed acute lymphoblastic leukemia. *Science* 2008;322:1377–1380.

References

1 Hanahan D, Weinberg RA. The hallmarks of cancer. *Cell* 2000; **100**: 57–70.
2 Hahn WC, Weinberg RA. Modelling the molecular circuitry of cancer. *Nat Rev Cancer* 2002; **2**: 331–41.
3 Calabretta B, Perrotti D. The biology of CML blast crisis. *Blood* 2004; **103**: 4010–22.
4 Mullighan CG, Goorha S, Radtke I *et al.* Genome-wide analysis of genetic alterations in acute lymphoblastic leukaemia. *Nature* 2007; **446**: 758–64.
5 Mullighan CG, Miller CB, Radtke I *et al.* BCR-ABL1 lymphoblastic leukaemia is characterized by the deletion of Ikaros. *Nature* 2008; **453**: 110–4.
6 Clarke MF, Dick JE, Dirks PB *et al.* Cancer stem cells – perspectives on current status and future directions: AACR Workshop on cancer stem cells. *Cancer Res* 2006; **66**: 9339–44.
7 Wakabayashi Y, Inoue J, Takahashi Y *et al.* Homozygous deletions and point mutations of the Rit1/Bcl11b gene in γ-ray induced mouse thymic lymphomas. *Biochem Biophys Res Commun* 2003; **301**: 598–603.
8 Kominami R, Niwa O. Radiation carcinogenesis in mouse thymic lymphomas. *Cancer Sci* 2006; **97**: 575–81.
9 Kaminura K, Mishim O, Ohi H *et al.* Haploinsufficiency of Bcl11b for suppression of lymphomagenesis and thymocyte development. *Biochem Biophys Res Commun* 2007; **355**: 538–42.
10 Nagel S, Kaufmann M, Drexler HG, MacLeod RA. The cardiac homeobox gene NKX2-5 is deregulated by juxtaposition with BCL11B in pediatric T-ALL cell lines via a novel t(5;14)(q35.1;q32.2). *Cancer Res* 2003; **63**: 5329–34.
11 MacLeod RA, Nagel S, Kaufmann M, Janssen JW, Drexler HG. Activation of HOX11L2 by juxtaposition with 3'-BCL11B in an acute lymphoblastic leukemia cell line (HPB-ALL) with t(5;14)(q35;q32.2). *Genes Chromosomes Cancer* 2003; **37**: 84–91.
12 Przybylski GK, Dik WA, Wanzeck J *et al.* Disruption of the BCL11B gene through inv(14)(q11.2q32.31) results in the expression of BCL11B-TRDC fusion transcripts and is associated with the absence of wild-type BCL11B transcripts in T-ALL. *Leukemia* 2005; **19**: 201–8.
13 Wakabayashi Y, Watanabe H, Inoue J *et al.* Bcl11b is required for differentiation and survival of αβT lymphocytes. *Nat Immunol* 2003; **4**: 533–9.
14 Inoue J, Kanefuji T, Okazuka K, Watanabe H, Mishima Y, Kominami R. Expression of TCRβ partly rescues developmental arrest and apoptosis of αβT cells in Bcl11b-/- mice. *J Immunol* 2006; **176**: 5871–9.
15 Arlotta P, Molyneaux BJ, Chen J, Inoue J, Kominami R, Macklis JD. Neuronal subtype-specific genes that control corticospinal motor neuron development in vivo. *Neuron* 2005; **45**: 207–21.
16 Golonzhka O, Liang X, Messaddeq N *et al.* Dual role of COUP-TF-interacting protein 2 in epidermal homeostasis and permeability barrier formation. *J Invest Dermatol* 2008; **129**: 1459–70.
17 Golonzhka O, Metzger D, Bornert JM *et al.* Ctip2/Bcl11b controls ameloblast formation during mammalian odontogenesis. *Proc Natl Acad Sci USA* 2009; **106**: 4278–83.
18 Avurum Albu DI, Feng D, Bhattacharya D *et al.* BCL11B is required for positive selection and survival of double-positive thymocytes. *J Exp Med* 2007; **204**: 3003–15.
19 Okazuka K, Wakabayashi Y, Kashihara M *et al.* p53 prevents maturation of T cell development to the immature CD4-CD8+ stage in Bcl11b-/- mice. *Biochem Biophys Res Commun* 2005; **328**: 545–9.
20 Fischer A, Malissen B. Natural and engineered disorders of lymphocyte development. *Science* 1998; **280**: 237–43.
21 Gounari F, Aifantis I, Khazaie K *et al.* Somatic activation of beta-catenin bypasses pre-TCR signaling and TCR selection in thymocyte development. *Nat Immunol* 2001; **2**: 863–9.
22 Xu Y, Banerjee D, Huelsken J, Birchmeier W, Sen JM. Deletion of beta-catenin impairs T cell development.Nat Immunol. *Nat Immunol* 2003; **4**: 1177–82.
23 Staal FJ, Clevers HC. Wnt signaling in the thymus. *Curr Opin Immunol* 2003; **15**: 204–8.
24 Ohi H, Mishima Y, Kamimura K, Maruyama M, Sasai K, Kominami R. Multi-step lymphomagenesis deduced from DNA changes in thymic lymphomas and atrophic thymuses at various times after γ-irradiation. *Oncogene* 2007; **26**: 5280–9.
25 Yamamoto T, Morita S, Go R *et al.* Clonally expanding thymocytes having lineage capability in g-ray induced mouse strophic thymus. *Int J Radiat Oncol Biol Phys* (in press).
26 Xu M, Sharma A, Wiest DL, Sen JM. Pre-TCR-induced β-catenin facilitates transversal through β-selection. *J Immunol* 2009; **182**: 751–8.
27 Xu M, Sharma A, Hossain MZ, Wiest DL, Sen JM. Sustained expression of pre-TCR induced beta-catenin in post-beta-selection thymocytes blocks T cell development. *J Immunol* 2009; **182**: 759–65.
28 Weerkamp F, Baert MR, Naber BA *et al.* Wnt signaling in the thymus is regulated by differential expression of intracellular signaling molecules. *Proc Natl Acad Sci USA* 2006; **103**: 3322–6.
29 Carleton M, Haks MC, Smeele SA *et al.* Early growth response transcription factors are required for development of $CD4^-CD8^-$ thymocytes to the $CD4^+CD8^+$ stage. *J Immunol* 2002; **168**: 1649–58.
30 Xi H, Kersh GJ. Early growth response gene 3 regulates thymocyte proliferation during the transition from $CD4^-CD8^-$ to $CD4^+CD8^+$. *J Immunol* 2004; **172**: 964–71.
31 Aifantis I, Gounari F, Scorrano L, Borowski C, von Boehmer H. Constitutive pre-TCR signaling promotes differentiation through Ca^{2+} mobilization and activation of NF-kappaB and NFAT. *Nat Immunol* 2001; **2**: 403–9.
32 Engel I, Murre C. E2A proteins enforce a proliferation checkpoint in developing thymocytes. *EMBO J* 2004; **23**: 202–11.
33 Gregorieff A, Clevers H. Wnt signaling in the intestinal epithelium: from endoderm to cancer. *Genes Dev* 2005; **19**: 877–90.
34 Guo Z, Dose M, Kovalovsky D *et al.* Beta-catenin stabilization stalls the transition from double-positive to single-positive stage and predisposes thymocytes to malignant transformation. *Blood* 2007; **109**: 5463–72.
35 Ioannidis V, Beermann F, Clevers H, Held W. The β-catenin-TCF-1 pathway ensures $CD4^+CD8^+$ thymocyte survival. *Nat Immunol* 2001; **2**: 691–7.
36 Mullighan CG, Phillips LA, Su X *et al.* Genomic analysis of the clonal origins of relapsed acute lymphoblastic leukemia. *Science* 2008; **322**: 1377–80.

Association of visceral fat accumulation and plasma adiponectin with rectal dysplastic aberrant crypt foci in a clinical population

Hirokazu Takahashi,[1,5] Tetsuji Takayama,[2] KyokoYoneda,[1] Hiroki Endo,[1] Hiroshi Iida,[1] Michiko Sugiyama,[1] Koji Fujita,[1] Masato Yoneda,[1] Masahiko Inamori,[1] Yasunobu Abe,[1] Satoru Saito,[1] Koichiro Wada,[3] Hitoshi Nakagama[4] and Atsushi Nakajima[1]

[1]Gastroenterology Division, Yokohama City University Graduate School of Medicine, Yokohama, Kanagawa 236-0004; [2]Gastroenterology Division, University of Tokushima Faculty of Medicine, Tokushima 770-8503; [3]Department of Pharmacology, School of Dentistry, Osaka University, Osaka 565-0871; [4]Biochemistry Division, National Cancer Center Research Institute, Tokyo 104-0045, Japan

(Received June 21, 2008/Revised August 31, 2008/Accepted September 5, 2008/Online publication October 23, 2008)

The association between obesity and the risk of colorectal cancer (CRC) cannot be easily evaluated because CRC itself is associated with a gradual loss of bodyweight. Aberrant crypt foci (ACF) can be classified as dysplastic ACF or non-dysplastic ACF by magnifying colonoscopy, and dysplastic ACF are thought to be a biomarker of CRC. Ninety-four participants who underwent colonoscopy at Yokohama City University Hospital, Japan, were enrolled in the current study. We detected 557 ACF, including 67 dysplastic ACF (12.0%). Univariate regression analysis was conducted to determine correlations between the number of dysplastic ACF and various potential risk factors, including patient age, waist circumference, body mass index, visceral fat area (VFA), and plasma adiponectin level. The results of multiple regression analysis revealed that the number of dysplastic ACF correlated with age (correlation coefficient $r = 0.212$, $P = 0.0383$) and plasma adiponectin level ($r = -0.201$, $P = 0.0371$), even after adjustments for sex, waist circumference, body mass index, and VFA. Our univariate correlation analysis data showed a significant correlation with the number of dysplastic ACF with VFA ($r = 0.238$, $P = 0.0209$), no correlation with subcutaneous fat area, and an inverse correlation with the plasma level of adiponectin ($r = -0.258$, $P = 0.0118$). Thus, our results suggest that aging and visceral fat accumulation could correlate moderately with colorectal carcinogenesis. The novelty of our study lies in the finding that visceral fat accumulation and a low plasma adiponectin level may promote colorectal carcinogenesis; therefore, these obesity-related parameters may serve as novel targets for CRC prevention. (*Cancer Sci* 2009; 100: 29–32)

Obesity and its associated visceral fat accumulation have been reported to be linked to an elevated risk of cardiovascular disease, diabetes mellitus, and mortality, and these complications are rapidly becoming significant problems.[1,2] Visceral adipose tissue is not only fat storage tissue, but also a metabolically active organ secreting many adipocytokines, such as adiponectin.[3] Obesity is reportedly an important risk factor for CRC.[4] CRC has high mortality and morbidity rates, and its prevalence has been increasing.[5,6] The precise risk factors for CRC remain unclear, although a family history and several dietary and lifestyle factors have been proposed to be involved.[7]

The association between obesity and the risk of CRC cannot be easily evaluated because of the confounding effect of bodyweight loss with CRC. Therefore, we sought to identify a biomarker for risk assessment and monitoring of CRC. ACF, which were first discovered in mice treated with azoxymethane,[8] have been clearly shown to be precursor lesions of CRC, and are now established as a biomarker of the risk of CRC in azoxymethane-treated mice and rats.[9] In humans, ACF can be classified as dysplastic or non-dysplastic through the use of magnifying colonoscopy.[10] ACF have not been firmly established to be precursors of CRC; however, dysplastic ACF could possibly serve as a biomarker of the risk of CRC. Previous studies have reported that individuals with CRC have more ACF than those without CRC, therefore dysplastic ACF represent potential clinical precursors of CRC and colorectal adenoma.[11–14] Recently, an association was suggested to exist between obesity and the risk of CRC.[15,16] However, the relationship between obesity and ACF remains unclear. Therefore, the current study in a clinical population aimed to investigate the relationship between various obesity-associated parameters and rectal dysplastic ACF.

Patients and Methods

Study population. We prospectively evaluated 94 subjects recruited from the population of healthy individuals who underwent colonoscopy at Yokohama City University Hospital, Japan. The exclusion criteria included: presence of contraindications to colonoscopy; current or past non-steroidal anti-inflammatory drug use including aspirin; family history of CRC; or history of adenoma, carcinoma, familial adenomatous polyposis, inflammatory bowel disease, or radiation colitis. Subjects with a history of colectomy, gastrectomy, or colorectal polypectomy, and those treated with daily insulin self-injection or sulfonylurea for diabetes mellitus, were also excluded. In order to investigate the influence of obesity on colorectal carcinogenesis, patients with colorectal adenoma or carcinoma at the time of colonoscopy were also excluded from the study. Written informed consent was obtained from all subjects prior to their participation. The study protocol was approved by the Yokohama City University Hospital Ethics Committee.

Collection and analysis of blood samples for adiponectin level. Blood samples were obtained in the morning on the day of colonoscopy after overnight fasting. Plasma adiponectin levels were measured by enzyme-linked immunosorbent assay of the total forms of human adiponectin (SRL Co., Tokyo, Japan).

Magnifying colonoscopy for identification of ACF. Participants' bowel preparation for the colonoscopy was carried out using

[5]To whom correspondence should be addressed.
E-mail: hirokazu@med.yokohama-cu.ac.jp
Abbreviations: ACF, aberrant crypt foci; BMI, body mass index; CRC, colorectal cancer; CT, computed tomography; SFA, subcutaneous fat area; TFA, total fat area; VFA, visceral fat area.

doi: 10.1111/j.1349-7006.2008.00994.x

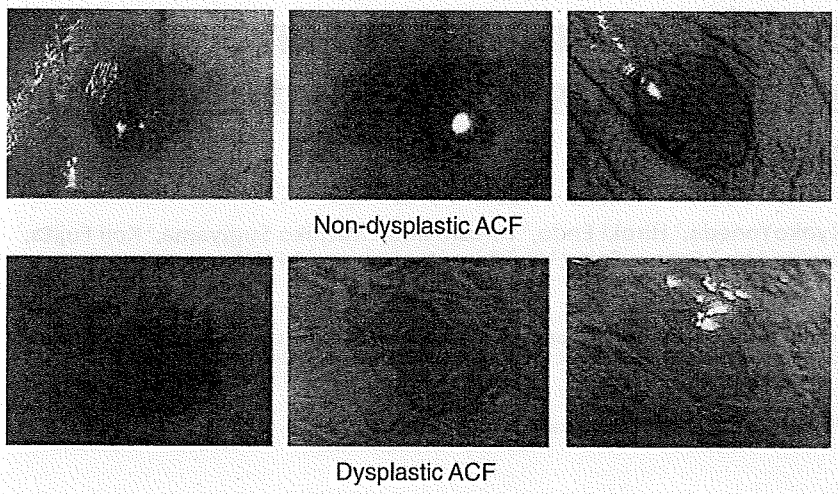

Fig. 1. Typical features of non-dysplastic and dysplastic aberrant crypt foci (ACF) on magnifying colonoscopy after methylene blue staining.

polyethylene glycol solution. A Fujinon EC-490ZW5/M colonoscope was used for the magnifying colonoscopy (Fujinon Toshiba ES Systems, Tokyo, Japan). Total colonoscopy was carried out before imaging of rectal ACF. Subsequently, 0.25% methylene blue was applied to the mucosa with a spray catheter. Aberrant crypts were distinguished from normal crypts by their deeper staining and larger diameter, and the number of ACF in the rectum was counted. This counting was conducted in the lower rectal region, extending from the middle Houston valve to the dentate line, based on the results of a previous study.[10] All ACF were recorded photographically and evaluated by two independent observers who were unaware of the subjects' clinical histories.

Criteria used for endoscopic diagnosis. ACF were defined as lesions in which the crypts were more darkly stained with methylene blue than normal crypts and had larger diameters, often with oval or slit-like lumens and a thicker epithelial lining.[17–20] Dysplastic ACF were defined as crypts in which each lumen was compressed or not distinct, with an epithelial lining that was much thicker than that of normal surrounding crypts. Non-dysplastic ACF were classified as hyperplastic or non-hyperplastic.[10]

Measurement of VFA and SFA. BMI was calculated using the following equation: bodyweight (kg)/(height [m]^2). Intra-abdominal adipose tissue was assessed, as described previously by measuring the VFA, SFA, TFA, and waist circumference from CT images at the level of the umbilicus.[4,10] All CT scans were carried out with the subjects in the supine position. The borders of the intra-abdominal cavity were outlined on the CT images, and the VFA was quantified using Fat Scan software (N2 System Corporation, Kobe, Japan).

Statistical analysis. We examined the associations between the risk factors for CRC and the number of dysplastic ACF. All data were expressed as mean ± SD, unless otherwise indicated. The relationships between the number of dysplastic ACF and relevant covariates were examined by univariate regression analysis, and standardized correlation coefficients were determined using Stat View software (SAS Institute, Cary, NC, USA). Multiple regression analysis was carried out to assess the relationship between the number of dysplastic ACF and potentially associated variables, and to determine the standardized correlation coefficients. The dependent variable was the number of dysplastic ACF, and the independent variables were age, sex, VFA, and plasma adiponectin level. Waist circumference and BMI were excluded from this analysis because these factors have a high correlation with VFA. P-values < 0.05 were considered to denote statistical significance.

Results

Colonoscopic features of ACF. A total of 557 ACF, including 67 dysplastic ACF, were counted by magnifying colonoscopy in the 94 patients. The aberrant crypts were larger, thicker, and more darkly stained than the normal crypts. Dysplastic ACF and non-dysplastic ACF accounted for 12.0% (67 of 557) and 88.0% (490 of 557) of the total, respectively. The number of subjects with dysplastic ACF was 34, and the number with non-dysplastic ACF was 76. In the lesions detected by magnifying colonoscopy, the size (i.e. median number of crypts ± SD) per ACF was 15.1 ± 10.4 and per dysplastic ACF was 8.5 ± 11.8. The average number of composition crypts per ACF was 93.2 ± 124.3 and per dysplastic ACF was 16.3 ± 26.2. In the 94 patients, the mean total number of ACF (non-dysplastic and dysplastic) per patient was 5.92 ± 6.50, and the mean number of dysplastic ACF per patient was 0.71 ± 1.16. The typical colonoscopic features of dysplastic and non-dysplastic ACF are shown in Figure 1.

Patient characteristics. The clinical characteristics of the study participants are shown in Table 1. The mean age was 65.1 ± 10.8 years, and there were 48 men and 46 women. The mean waist circumference, BMI, TFA, VFA, SFA, and plasma adiponectin level were 86.3 ± 10.0 cm, 23.3 ± 3.1 kg/m^2, 200.8 ± 91.4 cm^2, 83.9 ± 50.1 cm^2, 116.7 ± 60.4 cm^2, and 11.0 ± 5.6 μg/mL, respectively.

Univariate regression analysis: Correlations between risk factors for CRC and the number of dysplastic ACF. Age correlated significantly with the number of dysplastic ACF, as shown in Table 2 (r = 0.232, P = 0.0242). Sex showed no correlation with the number of dysplastic ACF. All of the obesity parameters, except SFA (r = –0.001, P = 0.9979), correlated significantly with the number of dysplastic ACF, as follows: waist circumference (r = 0.225, P = 0.0293), BMI (r = 0.307, P = 0.0325), and VFA (r = 0.238, P = 0.0209). The plasma level of adiponectin showed a significant inverse correlation with the number of dysplastic ACF (r = – 0.258, P = 0.0118). Age was the only parameter that correlated significantly with the number of non-dysplastic ACF (r = 0.218, P = 0.0336), which were much more abundant than dysplastic ACF in the study subjects.

Multiple regression analysis: Correlations between risk factors for CRC and the number of dysplastic ACF. The results of the multiple regression analysis are shown in Table 3. After adjustments for sex, waist circumference, BMI, and VFA, the parameters of age and plasma adiponectin level still correlated significantly with the number of dysplastic ACF (P = 0.0383 and P = 0.0371, respectively).

doi: 10.1111/j.1349-7006.2008.00994.x

Table 1. Clinical characteristics of study participants

Characteristic	Overall	Subjects with non-dysplastic ACF	Subjects with dysplastic ACF
Number	94	76	34
Age (years)	65.1 ± 10.8	66.3 ± 10.1	66.2 ± 8.1
Sex (male : female)	48:46	43:33	21:13
Waist circumference (cm)	86.3 ± 10.0	86.0 ± 10.5	88.4 ± 11.2
Body mass index (kg/m²)	23.3 ± 3.1	23.3 ± 3.2	24.2 ± 3.0
Total fat area (cm²)	200.8 ± 91.4	199.5 ± 95.7	222.0 ± 96.0
Visceral fat area (cm²)	83.9 ± 50.1	86.3 ± 51.6	103.6 ± 52.6
Ssubcutaneous fat area (cm²)	116.7 ± 60.4	112.9 ± 60.8	117.8 ± 58.4
Plasma adiponectin (μg/mL)	11.0 ± 5.6	11.3 ± 5.8	9.4 ± 4.3

Data are expressed as mean ± SD. ACF, aberrant crypt foci.

Table 2. Univariate correlation analysis: Correlations between the number of non-dysplastic or dysplastic aberrant crypt foci (ACF) and the risk factors for colorectal cancer

Risk factor	Non-dysplastic ACF		Dysplastic ACF	
	r	*P*	*r*	*P*
Age	0.218	0.0336*	0.232	0.0242*
Sex	0.109	0.2928	0.087	0.4069
Waist circumference	0.076	0.4651	0.225	0.0293*
Body mass index	0.169	0.1011	0.307	0.0325*
Total fat area	0.126	0.2257	0.135	0.1941
Visceral fat area	0.137	0.1868	0.238	0.0209*
Subcutaneous fat area	0.078	0.4560	−0.001	0.9979
Plasma adiponectin	−0.019	0.8538	−0.258	0.0118*

Age, waist circumference, body mass index, visceral fat area, and plasma adiponectin level correlated with the number of dysplastic ACF.
*$P < 0.05$.

Table 3. Multiple regression analysis: Correlations between the number of dysplastic aberrant crypt foci and the risk factors for colorectal cancer

Risk factor	Correlation coefficient	*P*
Age	0.212	0.0383*
Sex	0.038	0.7141
Waist circumference	−0.152	0.4508
Body mass index	0.249	0.1618
Visceral fat area	0.089	0.5807
Plasma adiponectin	−0.201	0.0371*

R^2 for the entire model = 0.368.
After adjustments for sex, waist circumference, body mass index, and visceral fat area, the parameters of age and plasma adiponectin level still correlated with the number of dysplastic aberrant crypt foci.
*$P < 0.05$.

Discussion

In the present study a total of 557 ACF were counted in the 94 patients, and we demonstrated a significant correlation between the number of dysplastic ACF and the VFA, and a significant inverse correlation between the number of dysplastic ACF and the plasma adiponectin level. Age was also associated with the number of ACF, that is, the number of dysplastic and non-dysplastic ACF increased with age. CRC is thought to progress through several morphological stages, from the formation of polyps to the onset of malignant change.[21] Genetic alterations, including mutations in the *K-ras*, *p53*, and *APC* genes, have been reported to be associated with the disease progression.[22] The *K-ras* mutation has also been reported in human ACF.[23] Therefore, the increased risk of ACF formation with age may be influenced mainly by these genetic alterations. Sex showed no correlation with the number of dysplastic ACF in the present study; however, the incidence of CRC is lower in women than in men.[24,25] It has been suggested that the initiation of dysplastic ACF is comparable in men and women, but thereafter tumor progression differs because visceral fat accumulation is higher in men than woman. This visceral fat accumulation may affect tumor progression.

Waist circumference has often been suggested to be associated with VFA. Consistent with this suggestion, our data showed that both waist circumference and VFA were associated with the number of dysplastic ACF. Recent reports have suggested that obesity may be associated with a high risk of CRC.[4] Several studies have shown that increased BMI is associated with an increased risk of CRC.[26] The importance of the size of ACF has been reported,[27] and the correlation between size, measured as the median number of crypts per both non-dysplastic ACF and dysplastic ACF, and risk factors was analyzed. The correlation between the median number of crypts per ACF and any risk factors had almost the same result as the number of ACF (data not shown). Our data showed a direct correlation between the VFA and the number of dysplastic ACF, and an inverse correlation between the plasma adiponectin level and the number of dysplastic ACF (Table 2). A previous study showed that the *K-ras* gene was mutated in 50–60% of patients with dysplastic ACF,[10] thus genetic alterations were already underway. Visceral fat correlated with dysplastic ACF in the current study, and another study showed that increased visceral adiposity was a significant predictor of lower rates of disease-free survival in patients with resectable colorectal cancer,[28] suggesting that visceral fat plays an important role in colorectal carcinogenesis and progression. Visceral fat tissue is known to be an endocrine organ that secretes adiponectin, which has an inverse relationship with obesity and visceral fat.[29] We carried out multiple regression analysis to assess whether plasma adiponectin may be a risk factor for dysplastic ACF growth, independent of the effects of obesity. If dysplastic ACF are a biomarker of the risk of colorectal adenoma and CRC, then some factors associated with the risk of CRC may also influence the number of dysplastic ACF. Very little is known about the factors that initiate or promote the growth of dysplastic ACF in humans. Our results suggest that plasma adiponectin levels are inversely associated with the number of ACF, and that visceral fat may be associated directly with ACF and thus could be a risk factor for the early stage of colorectal carcinogenesis.

There are many reports on the existence of relationships between the risk of CRC and exercise, energy use, glycemic index, and food choices and dietary constituents.[30–32] These factors affect each other, therefore it is difficult to evaluate the relationship between any one factor and the risk of CRC. Obesity

is thought to result from many of these factors. It is also thought that aging, visceral fat, and adiponectin are important in CRC carcinogenesis. Further investigation is needed to elucidate the mechanisms that affect these relationships and the impact on the development of CRC.

The novelty of our study lies in our use of dysplastic ACF as a biomarker for risk of CRC to show that visceral fat accumulation and low plasma adiponectin level may affect colorectal carcinogenesis. Further studies should be conducted to clarify the role that visceral fat accumulation and reduced plasma adiponectin play in dysplastic ACF growth and whether these obesity-related parameters may serve as novel targets for CRC prevention.

Acknowledgments

We thank Machiko Hiraga for her technical assistance. This work was supported in part by a Grant-in-Aid for research on the Third Term Comprehensive Control Research for Cancer from the Ministry of Health, Labour, and Welfare, Japan to A.N., a grant from the National Institute of Biomedical Innovation to A.N., a grant from the Ministry of Education, Culture, Sports, Science, and Technology, Japan (KIBAN-B) to A.N., a grant from the Ministry of Education, Culture, Sports, Science, and Technology, Japan (WAKATE-B) to H.T., a research grant from the Princess Takamatsu Cancer Research Fund to A.N., and a grant for the 2007 Strategic Research Project (no. K19041) of Yokohama City University, Japan to H.T. and A.N.

References

1 Fujioka S, Matsuzawa Y, Tokunaga K *et al.* Contribution of intra-abdominal fat accumulation to the impairment of glucose and lipid metabolism in human obesity. *Metabolism* 1987; **36**: 54–9.
2 Kissebah AH, Vydelingum N, Murray R *et al.* Relation of body fat distribution to metabolic complications of obesity. *J Clin Endocrinol Metab* 1982; **54**: 254–60.
3 Park KG, Park KS, Kim MJ *et al.* Relationship between serum adiponectin and leptin concentrations and body fat distribution. *Diabetes Res Clin Pract* 2004; **63**: 135–42.
4 Giovannucci E, Aasherio A, Rimm EB *et al.* Physical activity, obesity, and risk for colon cancer and adenoma in men. *Ann Intern Med* 1995; **122**: 327–34.
5 Anderson WF, Umar A, Brawley OW. Colorectal carcinoma in black and white race. *Cancer Metastasis Rev* 2003; **22**: 67–82.
6 Rougier P, Mitry E. Epidemiology, treatment and chemoprevention in colorectal cancer. *Ann Oncol* 2003: **14**: ii3–5.
7 Garland C, Shekelle RB, Barrett-Connor E *et al.* Dietary vitamin D and calcium and risk of colorectal cancer: a 19-year prospective study in men. *Lancet* 1985; **1**: 307–9.
8 Bird RP. Observation and quantification of aberrant crypts in the murine colon treated with a colon carcinogen: preliminary findings. *Cancer Lett* 1987; **37**: 147–51.
9 Pretlow TP, O'Riordan MA, Somich GA *et al.* Aberrant crypts correlate with tumor incidence in F344 rats treated with azoxymethane and phytate. *Carcinogenesis* 1992; **13**: 1509–12.
10 Takayama T, Katsuki S, Takahashi Y *et al.* Aberrant crypt foci of the colon as precursors of adenoma and cancer. *N Engl J Med* 1998; **339**: 1277–84.
11 Nascimbeni R, Villanacci V, Mariani PP *et al.* Aberrant crypt foci in the human colon: frequency and histologic patterns in patients with colorectal cancer or diverticular disease. *Am J Surg Pathol* 1999; **23**: 1256–63.
12 Shpitz B, Bomstein Y, Mekori Y *et al.* Aberrant crypt foci in human colons: distribution and histomorphologic characteristics. *Hum Pathol* 1998; **29**: 469–75.
13 Adler DG, Gostout CJ, Sorbi D *et al.* Endoscopic identification and quantification of aberrant crypt foci in the human colon. *Gastrointest Endosc* 2002; **56**: 657–62.
14 Nucci MR, Robinson CR, Longo P *et al.* Phenotypic and genotypic characteristics of aberrant crypt foci in human colorectal mucosa. *Hum Pathol* 1997; **28**: 1396–407.
15 Gunter MJ, Leitzmann MF. Obesity and colorectal cancer: epidemiology, mechanisms and candidate genes. *J Nutr Biochem* 2006; **17**: 145–56.
16 Otake S, Takeda H, Suzuki Y *et al.* Association of visceral fat accumulation and plasma adiponectin with colorectal adenoma: evidence for participation of insulin resistance. *Clin Cancer Res* 2005; **11**: 3642–6.
17 Roncucci L, Stamp D, Medline A *et al.* Identification and quantification of aberrant crypt foci and microadenomas in the human colon. *Hum Pathol* 1991; **22**: 287–94.
18 Roncucci L, Medline A, Bruce WR. Classification of aberrant crypt foci and microadenomas in human colon. *Cancer Epidemiol Biomarkers Prev* 1991; **1**: 57–60.
19 Pretlow TP, Barrow BJ, Ashton WS *et al.* Aberrant crypts: putative preneoplastic foci in human colonic mucosa. *Cancer Res* 1991; **51**: 1564–7.
20 Pretlow TP, O'Riordan MA, Pretlow TG *et al.* Aberrant crypts in human colonic mucosa: putative preneoplastic lesions. *J Cell Biochem Suppl* 1992; **16**: 55–62.
21 Kinzler KW, Vogelstein B. Lessons from hereditary colorectal cancer. *Cell* 1996; **87**: 159–70.
22 Fearon ER, Vogelstein B. A genetic model for colorectal tumorigenesis. *Cell* 1990; **61**: 759–67.
23 Yuan P, Sun MH, Zhang JS *et al.* APC and K-ras gene mutation in aberrant crypt foci of human colon. *World J Gastroenterol* 2001; **7**: 352–6.
24 Gao RN, Neutel CI, Wai E. Gender differences in colorectal cancer incidence, mortality, hospitalizations and surgical procedures in Canada. *J Public Health* 2008; **30**: 194–201.
25 de Kok IM, Wong CS, Chia KS *et al.* Gender differences in the trend of colorectal cancer incidence in Singapore, 1968–2002. *Int J Colorectal Dis* 2008; **23**: 461–7.
26 Graham S, Marshall J, Haughey B *et al.* Dietary epidemiology of cancer of the colon in western New York. *Am J Epidemiol* 1988; **128**: 490–503.
27 Rudolph RE, Dominitz JA, Lampe JW *et al.* Risk factors for colorectal cancer in relation to number and size of aberrant crypt foci in humans. *Cancer Epidemiol Biomarkers Prev* 2005; **14**: 605–8.
28 Moon HG, Ju YT, Jeong CY *et al.* Visceral obesity may affect oncologic outcome in patients with colorectal cancer. *Ann Surg Oncol* 2008; **15**: 1918–22.
29 Arita Y, Kihara S, Ouchi N *et al.* Paradoxical decrease of an adipose-specific protein, adiponectin, in obesity. *Biochem Biophys Res Commun* 1999; **257**: 79–83.
30 Gerhardsson M, Floderus B, Norell SE. Physical activity and colon cancer risk. *Int J Epidemiol* 1988; **17**: 743–6.
31 Slattery ML, Benson J, Berry TD *et al.* Dietary sugar and colon cancer. *Cancer Epidemiol Biomarkers Prev* 1997; **6**: 677–85.
32 Reedy J, Haines PS, Steckler A *et al.* Qualitative comparison of dietary choices and dietary supplement use among older adults with and without a history of colorectal cancer. *J Nutr Educ Behav* 2005; **37**: 252–8.

doi: 10.1111/j.1349-7006.2008.00994.x

	C A S	1 5 4 6	B	Dispatch: 22.3.10	Journal: CAS	CE: Ulagammal
	Journal Name	Manuscript No.		Author Received:	No. of pages: 7	PE: Radhika

Bcl11b heterozygosity promotes clonal expansion and differentiation arrest of thymocytes in γ-irradiated mice

Rieka Go,[1] Satoshi Hirose,[1] Shinichi Morita,[1] Takashi Yamamoto,[1] Yoshinori Katsuragi,[1] Yukio Mishima[1,2] and Ryo Kominami[1,2,3]

[1]Department of Molecular Genetics, Graduate School of Medical and Dental Sciences; [2]Center for Transdisciplinary Research, Niigata University, Niigata, Japan

2 (Received November 19, 2009/Revised February 17, 2010/Accepted February 20, 2010/Accepted manuscript online Xxxxxx xx Xxxx)

Bcl11b **encodes a zinc-finger transcription factor and functions as a haploinsufficient tumor suppressor gene. *Bcl11b*$^{KO/KO}$ mice exhibit differentiation arrest of thymocytes during β-selection as has been observed with other mouse models involving knockouts of genes in the Wnt/β-catenin signaling pathway. Recurrent chromosomal rearrangement at the *BCL11B* locus occurs in human T-cell leukemias, but it is not clear how such rearrangement would contribute to lymphomagenesis. To address this issue, we studied clonal cell growth, cell number, and differentiation of thymocytes in *Bcl11b*$^{KO/+}$ mice at different time points following γ-irradiation. 1 Analysis of D-J rearrangement at the *TCRβ* locus and cell surface markers by flow cytometry revealed two distinct populations of clonally growing thymocytes. In one population, thymocytes share a common D-J rearrangement but retain the capacity to differentiate. In contrast, thymocytes in the second population have lost their ability to differentiate. Since the capacity to self renew and differentiate into multiple cell lineages are fundamental properties of adult stem cells, the differentiation competent population of thymocytes that we have isolated could potentially function as cancer stem cells. We also demonstrate increased expression of β-catenin, a well-known oncogenic protein, in *Bcl11b*$^{KO/+}$ thymocytes. Collectively, the *Bcl11b*$^{KO/+}$ genotype contributes to clonal expansion and differentiation arrest in part through an increase in the level of β-catenin. (*Cancer Sci* 2010)**

Cancer development is a complex, multistep process involving the acquisition of capabilities of cell autonomous proliferation and resistance to apoptosis.[1] This could be a consequence of a sequence of 4–6 mutations that are associated with different stages of the tumor progression.[2] Leukemia and lymphoma are malignancies of hematopoietic cells, and chronic myelogenous leukemia (CML) is among the malignancies characterized with frequently having the *bcr/abl* chimeric gene.[3] A two-step process is seen from CML to a subset of acute lymphoblastic leukemia (ALL) bearing *bcr/abl*, an aggressive blast crisis phase.[3–5] This transition requires an arrest of differentiation. Interestingly, CML already possesses intrinsic self-renewal capability like adult tissue stem cells and differentiate to mature, nontumorigenic blood cells.[6]

Bcl11b is a haploinsufficient tumor suppressor gene that was isolated from analyses of γ-ray induced mouse thymic lymphomas.[7–9] *Bcl11b*$^{KO/+}$ mice are susceptible to the development of thymic lymphomas,[9] suggesting that loss or decrease of Bcl11b function contributes to lymphomagenesis. Recurrent chromosomal rearrangement at the human *BCL11B* locus has been reported in T-cell leukemias,[10–12] but the effects of the rearrangement are not clear. *Bcl11b* encodes a zinc-finger transcription factor that is expressed in thymocytes, neurons and other tissues.[13–17] *Bcl11b*$^{KO/KO}$ and *Bcl11b*$^{lox/lox}$ mice show differentiation arrest of thymocytes during β-selection[13,14] and positive selection,[18] respectively; the arrest in the former seen at CD4 and CD8 double-negative (DN) and immature CD8 single-positive (ISP) cell stages before the CD4 and CD8 double-positive (DP) cell stage.[13,14] *Bcl11b*$^{KO/+}$ mice exhibit a substantial impairment of thymocyte differentiation in mouse embryos, although not as profound as that in *Bcl11b*$^{KO/KO}$ animals.[19] The arrest during β-selection is seen in many gene-knockout mice,[20] including genes affecting Wnt/β-catenin signaling.[21–23] As with oncogenesis, differentiation arrest may be a mechanism through which Bcl11b deficiency contributes to tumor development. However, *Bcl11b*$^{KO/KO}$ mice also show thymocyte apoptosis, and this anti-apoptotic property of Bcl11b seems to contradict a predicted proapoptotic function of tumor suppressors. The differentiation arrest and apoptosis are at least in part due to the decrease of pre-TCR signaling.[13,14] 2

Identical rearrangements of the *TCRβ* locus are seen in thymic lymphomas and this establishes clonality of the lymphomas.[24] Our previous studies demonstrated that such identical rearrangements were also found in γ-ray induced mouse atrophic thymuses, indicating the existence of clonally expanded thymocytes.[24,25] A significant percentage of those thymuses exhibited allelic loss of *Bcl11b*. These findings raise the question of how and at which stage does the *Bcl11b* heterozygous genotype contributes to lymphoma development. Here we studied the effect of *Bcl11b*$^{KO/+}$ genotype on β-catenin expression and on clonal cell proliferation of thymocytes in γ-irradiated mice. Our results provide an implication that the genotype contributes to clonal cell expansion and differentiation arrest, and the contribution may, in part, occur through an increase in β-catenin expression.

Materials and Methods

Mice and induction of atrophic thymus. *Bcl11b*$^{KO/+}$ mice with a BALB/c background were generated as described.[13] MSM mice were kindly supplied from Dr Shiroishi, NIG (Mishima, Japan). *Bcl11b*$^{KO/+}$ mice were mated with MSM 3 mice and their progeny were subjected to γ-irradiation of 3 Gy at 8 or 10 weeks of age. Left and right thymic lobes were separately isolated at 30, 60, or 80 days after the irradiation and subjected to analyses. Mice used in this study were maintained under specific pathogen-free conditions in the animal colony of Niigata University. All animal experiments complied with the guidelines for animal experimentation from the University animal ethics committee.

[3]To whom correspondence should be addressed.
E-mail: rykomina@med.niigata-u.ac.jp

doi: 10.1111/j.1349-7006.2010.01546.x

Flow cytometry. Flow cytometric analysis was performed as previously described.[13] In brief, single cell suspensions of thymocytes were prepared from thymus and 1–2 × 10^6 cells were incubated with antibodies in phosphate-buffered saline containing 2% fetal calf serum and 0.2% NaN_3 for 20 min at 4°C. The monoclonal antibodies (mAbs) used were: anti-CD4-PerCP-Cy5.5 or -APC (RM4-5), anti-CD8-PE (53-6.7), anti-TCRβ-FITC (H57-597; BioLegend), anti-β-catenin-FITC (14; BD Biosciences, San Jose, CA, USA), and IL-7Rα-PE (SB/199, BioLegend). They were purchased from eBioscience. To prevent nonspecific binding of mAbs, we added CD16/32 (93; eBioscience) before staining with labeled mAbs. Dead cells and debris were excluded from the analysis by appropriate gating of FSC and SSC. Cells were analyzed by a FACScan (Becton-Dickinson) flow cytometer, and data were analyzed using the Flow-Jo software (Tree-Star).

For BrdU incorporation experiments, we injected mice intraperitoneally with 100 μL of BrdU solution (10 mg/mL) and thymus was isolated 1 h after. Thymocytes were prepared from the thymus and analyzed with the use of the BrdU Flow Kit (BD Pharmingen) according to the manufacturer's instructions. In brief, cells were suspended at a concentration of 1–2 × 10^6 cells/mL, fixed, permeabilized, treated with DNase to expose incorporated BrdU, and incubated with a murine anti-BrdU antibody for 20 min at room temperature. After washing, cells were resuspended in 1 mL of PBS containing 20 μL of the 7AAD solution. Cells were resuspended in staining buffer and analyzed with the FACScan flow cytometer.

DNA isolation and PCR analysis. DNA was isolated from brain, thymocytes, and thymic lymphomas using the DNeasy Tissue Kit (Qiagen). To determine D-J rearrangement patterns in the *TCRβ* locus, polymerase chain reaction (PCR) was performed as described.[24,25] Of allelic loss analysis at the *Bcl11b* locus, *D12Mit53* and *D12Mit279* markers were used for PCR as described previously.[7] The PCR reaction was processed through 32 cycles of 94°C for 30 s, 55°C for 30 s, and 72°C for 1 min in most cases. The products were analyzed by 8% polyacrylamide gel electrophoresis. PCR bands were stained with ethidium bromide and band intensities were quantitated with a Molecular Imager FX (Bio-Rad Laboratories, Hercules, CA, USA) to determine the allele ratio of BALB/c and MSM alleles or of MSM and BALB/c alleles.

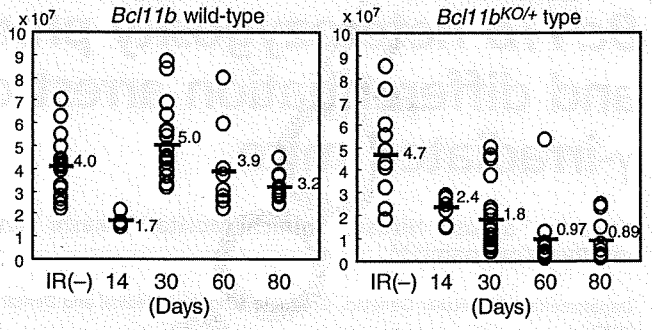

Fig. 1. Cell number in thymuses at various days after γ-irradiation. *Bcl11b*$^{+/+}$ mice, left; *Bcl11b*$^{KO/+}$ mice, right. Average cell number in *Bcl11b*$^{+/+}$ mice was 4.0, 1.7, 5.0, 3.9, and 3.2 × 10^7 cells for unirradiated, 14, 30, 60, and 80 days after irradiation, respectively. Average cell number in *Bcl11b*$^{KO/+}$ mice was 4.7, 2.4, 1.8, 0.97, and 0.89 × 10^7 cells for unirradiated, 14, 30, 60, and 80 days after irradiation, respectively.

Results

Decrease in the thymocyte number in γ-irradiated *Bcl11b*$^{KO/+}$ mice. We subjected 8-week-old *Bcl11b*$^{KO/+}$ and *Bcl11b*$^{+/+}$ mice to 3 Gy of γ-radiation and examined both left and right

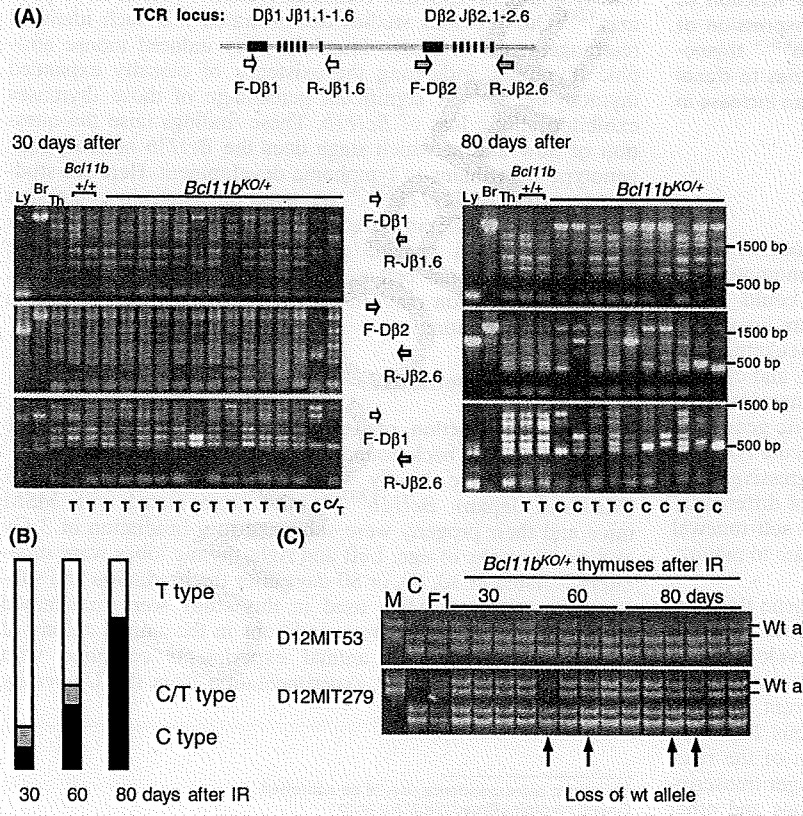

Fig. 2. Clonal growth of thymocytes in thymuses after γ-irradiation of 8-week-old *Bcl11b*$^{KO/+}$ mice. (A) D-J rearrangement patterns at the *TCRβ* locus in thymuses at 30 and 80 days after irradiation. The upper diagram shows part of the *TCRβ* locus and the relative location of PCR primers used. The lower panel shows gel electrophoresis of PCR products with three different sets of primers, F-Dβ1 and R-Jβ1.6 (top), F-Dβ2 and to-Jβ2.6 (middle), and F-Dβ1 and R-Jβ2.6 (bottom). T below the panel indicates T-type thymus that shows identical or similar rearrangement patterns to the control thymus, and C indicates C-type thymus that shows a few bands more prominent than the other bands or limited numbers of bands. C/T indicates C/T-type thymus between the T-type and C-type patterns. Size markers are shown at right. (B) Incidences of C- (black box), C/T- (gray box) and T-type (white box) thymuses in 30, 60, and 80 days after γ-irradiation in *Bcl11b*$^{KO/+}$ mice. (C) Allelic losses at the *Bcl11b* locus in irradiated thymuses. Two panels show polyacrylamide gel electrophoresis for PCR products of *D12Mit53* and *D12Mit279* primer pairs. Chromosomal location of *D12Mit53*, *Bcl11b*, and *D12Mit279* is 108.69, 109.15–24, 109.69 Mb from the centromere, respectively. We determined the allele ratio of BALB/c and MSM bands and judged the thymus as allelic loss-positive when the allele ratio was more than 2 or less than 0.5.

doi: 10.1111/j.1349-7006.2010.01546.x

lobes of the thymus separately at 14, 30, 60, and 80 days after irradiation (the respective thymic lobes are designated as 14-, 30-, 60-, and 80-day thymuses). The earliest time at which fully malignant thymic lymphomas were observed was approximately 100 days after irradiation.[7–9] Figure 1 shows the cell number in the thymuses. In *Bcl11b*$^{+/+}$ mice, the number at 14 days post radiation was not restored to the level in unirradiated mice but restored to the level or more at 30 days after. The cell number was maintained until 80 days after. On the other hand, *Bcl11b*$^{KO/+}$ mice showed impairment in the recovery of cellularity. The cell number at 30 days after was not restored to the normal level in most thymuses and the average was 1.8×10^7 in *Bcl11b*$^{KO/+}$ thymuses which was lower than 5.0×10^7 in *Bcl11b*$^{+/+}$ thymuses ($P < 0.0001$). Also, the cell number was not well maintained at 60 or 80 days after. These results suggest an impairment in the maintenance of thymocyte number in *Bcl11b*$^{KO/+}$ mice after γ-irradiation.

Clonal cell expansion. Clonality was determined by assaying specific V(D)J rearrangements with three primer sets designed for the *TCRβ* locus.[24,25] Figure 2(A) shows PCR patterns of 30- and 80-day thymuses. Unirradiated thymus (lane Th) gave six different bands corresponding to possible recombination sites between D and J regions by Dβ1-Jβ1, Dβ2-Jβ2, and Dβ1-Jβ2 probe sets and one band for germ-line DNA by the former two probe sets. On the other hand, thymic lymphoma DNA (Ly) gave one band only by the Dβ2-Jβ2 probe set used, indicating an identical rearrangement, and brain DNA (Br) gave the germ-line DNA band by Dβ1-Jβ1 and Dβ2-Jβ2 probe sets. Two of the 20 30-day thymuses in *Bcl11b*$^{KO/+}$ mice exhibited only a few bands or limited numbers of bands different from the normal thymus pattern, indicating the existence of clonally expanded thymocytes (C-type thymus). Most others showed rearrangement patterns identical or similar to the control thymus (classified as T-type thymus). There was one thymus that was classified as C/T-type thymus due to the difficulty of distinction between C- and T-type thymus. An additional experiment showed a consistent result, one C/T-type thymus detected in 12 30-day thymuses examined (data not shown). All 20 *Bcl11b*$^{+/+}$ mouse thymuses were T-type thymus (data not shown). On the other hand, the 60-day *Bcl11b*$^{KO/+}$ thymuses showed two C-type and four C/T-type thymuses in 10 thymuses examined, whereas the 80-day *Bcl11b*$^{KO/+}$ thymuses showed six C-type and two C/T-type thymuses in 10 thymuses examined (Fig. 2B). These indicate increase in the incidence of C-type thymus with the time after irradiation. Those results suggest that *Bcl11b*$^{KO/+}$ genotype promotes the development of clonally expanding thymocytes in γ-irradiated mice.

We examined loss of the wild-type *Bcl11b* allele in C- and T-type thymuses using MIT microsatellite markers flanking the *Bcl11b* locus (Fig. 2C). Of the 40 *Bcl11b*$^{KO/+}$ thymuses examined, four exhibited loss of the wild-type allele. All of these were C-type thymus. Their average cell number was as low as 0.20×10^7, and this decrease may be due to a loss of Bcl11b function because *Bcl11b*$^{KO/KO}$ thymocytes exhibit profound apoptosis.[13]

Cell cycle and cell size. We examined the cell cycle distribution of irradiated thymocytes that were isolated from mice at 1 h after intraperitoneal injection of BrdU. We determined the percentage of S-phase cells, size of G1-phase cells, and percentage of a fraction containing large thymocytes in the G1 phase. Figure 3(A) shows examples of flow cytometric analysis. The large cells in the G1 phase (indicated by a horizontal bar) were designated as middle-sized cells because their size was between the size of normal G1 cells (small size) and the size of S phase cells (large size). Figure 3(B) summarizes the percentage of S-phase cells at the vertical axis and the percentage of the middle-sized G1 cells at the horizontal axis in the two groups of 30-day thymuses and 60- plus 80-day thymuses. As for the 30-day thymuses, the percentage of S-phase cells or middle-sized G1 cells did not much differ between *Bcl11b*$^{KO/+}$ and *Bcl11b*$^{+/+}$ thymuses except for one thymus. On the other hand, there were eight *Bcl11b*$^{KO/+}$ thymuses possessing more than 20% middle-sized G1 cells among the 60/80-day *Bcl11b*$^{KO/+}$ thymuses, which were all C type. They showed a considerable variation in the percentage of the S phase. The middle-sized thymocytes may be related with premalignancy because cell-size enlargement is a characteristic of thymic lymphomas.[24] Those thymocytes are probably cells pausing at the G1 stage, and growing and progressing toward the S phase.

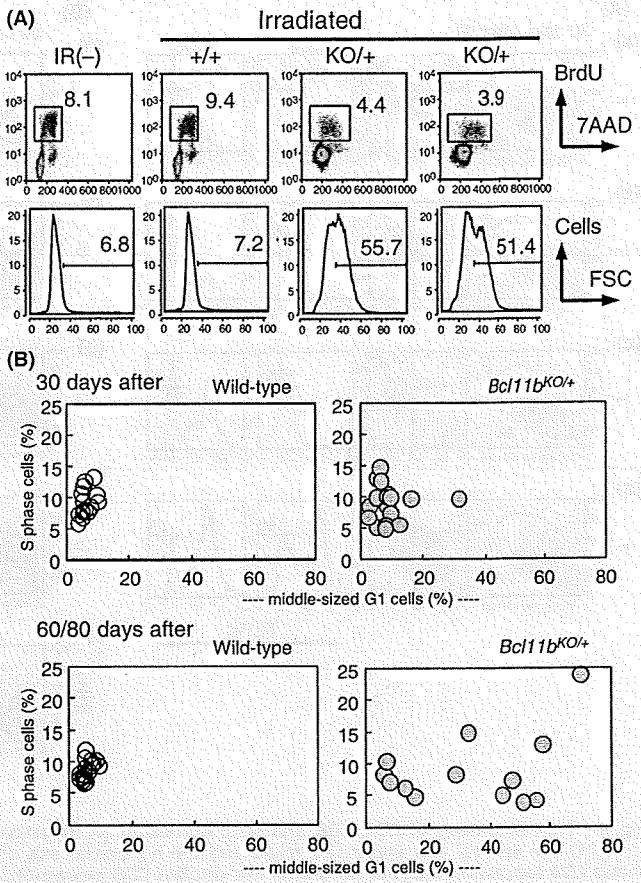

Fig. 3. Cell proliferation and cell size. (A) Flow cytometry of cell cycle in unirradiated and irradiated thymuses. (upper) The vertical axis shows BrdU incorporation levels and the horizontal axis displays 7-AAD staining for DNA contents. A square marks a fraction of thymocytes in the S-phase, and the number gives the percentage of S-phase cells. (lower) The vertical axis shows the cell number and the horizontal axis displays FSC values reflecting the cell size in G1-phase thymocytes. The bar shows a fraction of thymocytes in large size (middle-sized G1 cells) and the number above the bar indicates the percent of those thymocytes. The percentage was determined in each thymus by the criterion where the percentage in normal thymus was set to approximately 5% of the FSC value. (B) The vertical axis shows the percentage of S-phase cells and the horizontal axis displays the percentage of middle-sized G1 cells. Thirty-day thymuses, upper; groups of 60- and 80-day thymuses, lower; *Bcl11b*$^{+/+}$ thymuses, left; *Bcl11b*$^{KO/+}$ thymuses, right.

Differentiation arrest. Thymocytes from *Bcl11b*$^{KO/KO}$ mice show differentiation arrest at DN and ISP stages to lack DP cells,[13,14] and hence C-type thymocytes or possibly T-type thymocytes may exhibit differentiation arrest. We examined 12 30-day and 10 80-day thymuses with flow cytometry using CD4, CD8, and TCRβ cell surface markers (Fig. 4A,B). We defined

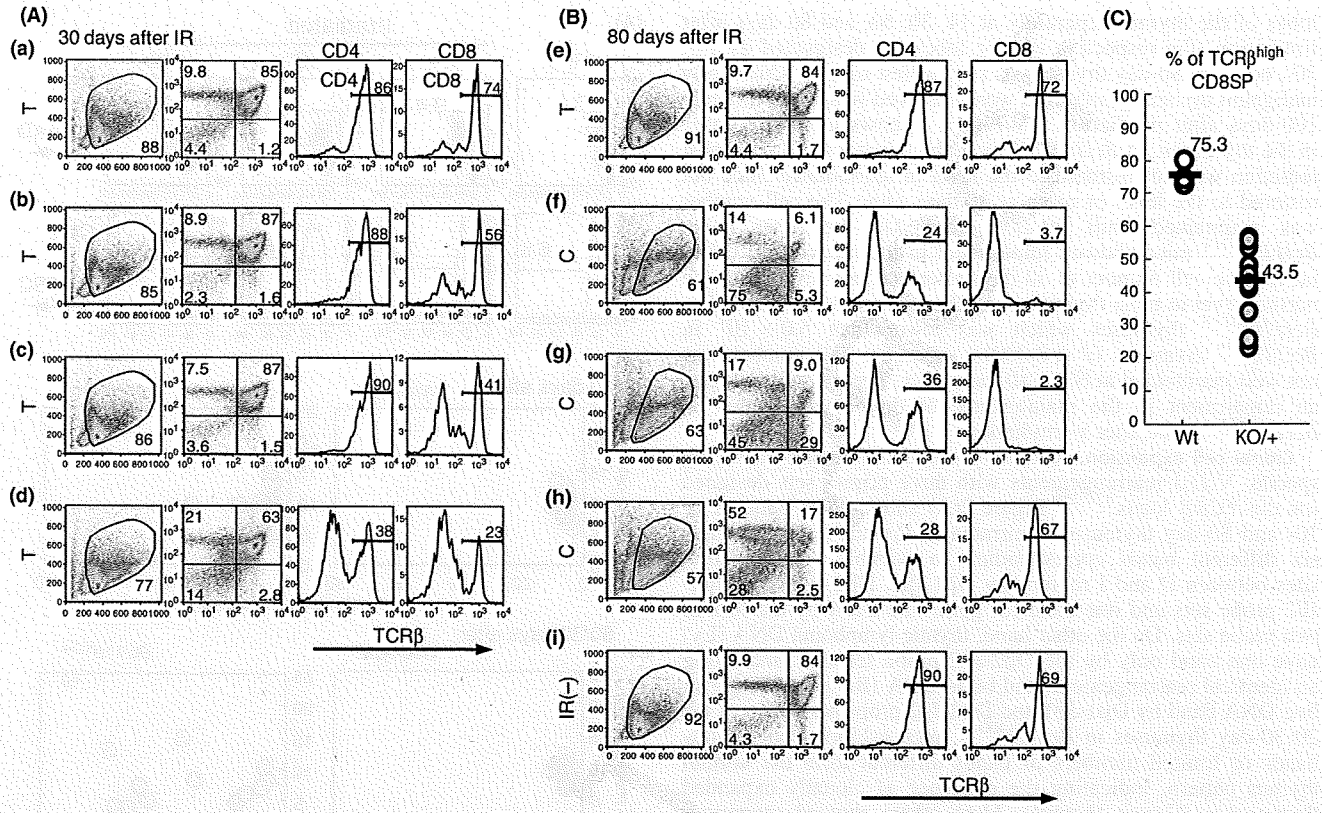

Fig. 4. Flow cytometry of CD4, CD8, and TCRβ expression on thymocytes. Thymocytes at 30 days (A) and 80 days (B) after irradiation. (from left to right) The vertical axis shows SSC values and the horizontal axis displays FSC values (the gated region marked by a circle); the vertical axis shows CD4 expression and the horizontal axis displays CD8 expression; the vertical axis shows cell number and the horizontal axis displays TCRβ expression of thymocytes in the CD4 quadrant; the vertical axis shows cell number and the horizontal axis displays TCRβ expression of thymocytes in the CD8 quadrant. (a) in (A) is a thymus in irradiated *Bcl11b*$^{+/+}$ mice and (b–d) are thymuses in irradiated *Bcl11b*$^{KO/+}$ mice. All four thymuses are T type. (e–h) in (B) are irradiated *Bcl11b*$^{KO/+}$ mice and (i) is an unirradiated *Bcl11b*$^{KO/+}$ mice. (e) is T-type and (f–h) are C-type thymuses. (C) The percentage of TCRβ^{high} CD8SP thymocytes in *Bcl11b*$^{+/+}$ (75.3%) and *Bcl11b*$^{KO/+}$ (43.5%) mice.

the gated region on the FSC *versus* SSC dot plot to exclude debris and dead cells. Although the cell percentage in the gated region did not much differ in the 30-day thymuses, it markedly differed among 80-day thymuses. The fraction of debris and dead cells increased in C- but not in T-type thymuses (data not shown). Analysis of CD4 and CD8 markers revealed that almost all T-type thymocytes of 30-day *Bcl11b*$^{KO/+}$ (also *Bcl11b*$^{+/+}$) mice except for one (d) showed a pattern similar to unirradiated normal thymus, mainly consisting of DP cells. However, analysis of TCRβ showed lower percentages of TCRβ^{high} mature CD8^{+} cells in *Bcl11b*$^{KO/+}$ thymocytes than *Bcl11b*$^{+/+}$ thymocytes (Fig. 4C). These together indicated a small impairment of differentiation in *Bcl11b*$^{KO/+}$ thymocytes. On the other hand, all eight C- and C/T-type thymuses of 80-day *Bcl11b*$^{KO/+}$ mice showed marked differentiation impairment. For instance, (f) in Figure 4(B) shows thymocytes at the DN fraction by CD4 and CD8 expression, and (g) and (h) show thymocytes mainly at the DN/ISP and CD4 fractions, respectively. CD4^{+} SP cells in (h) mostly showed low expression of the TCRβ protein, different from normal CD4^{+} SP cells. These results suggest that the *Bcl11b*$^{KO/+}$ genotype confers differentiation impairment of thymocytes in γ-irradiated mice.

In order to further study the relationship between clonal expansion and differentiation arrest, we subjected 10-week-old *Bcl11b*$^{KO/+}$ mice to 3-Gy γ-radiation and examined thymuses at 30 days after. This experimental condition was chosen based on the higher incidence (6/8, 75%) of C-type thymus observed in mice irradiated at this age and the decrease to 10% (2/20) when mice were irradiated at 4 weeks of age (data not shown). D-J rearrangement assay revealed C-type thymus in six of the 12 thymuses and T-type thymuses in the remaining six (Fig. 5A). The decrease in cell number was observed in *Bcl11b*$^{KO/+}$ mice as predicted, the average number being 1.25×10^{7}. On the other hand, the average of S-phase cells was as low as 4.0% in *Bcl11b*$^{KO/+}$ mice, and there was one C-type thymus possessing more than 20% middle-sized thymocytes. Figure 5(B) shows examples of flow cytometric analysis using CD4, CD8, and TCRβ markers. Of the six C-type thymuses, only two showed differentiation arrest (see b and c), and the remaining four C-type thymuses showed a normal differentiation pattern but lower expression of TCRβ (d and e). This indicated that thymocytes in the four C-type thymuses were capable of differentiating into mature cell types. This contrasts with the results of 80-day thymuses irradiated at 8 weeks of age: all C- and C/T-type thymuses showed impairment in the development of mature thymocytes. These results suggest a process from normally differentiating C-type thymocytes to differentiation-arrested C-type thymocytes in irradiated *Bcl11b*$^{KO/+}$ mice.

Elevation of β-catenin expression in *Bcl11b*$^{KO/+}$ thymocytes. During the flow cytometric analysis using CD4, CD8, and TCRβ markers, we noted a higher percentage of TCRβ^{-} CD8^{+} immature ISP cells and a lower percentage of DN cells in *Bcl11b*$^{KO/+}$ thymocytes (data not shown). The high ISP and low

doi: 10.1111/j.1349-7006.2010.01546.x

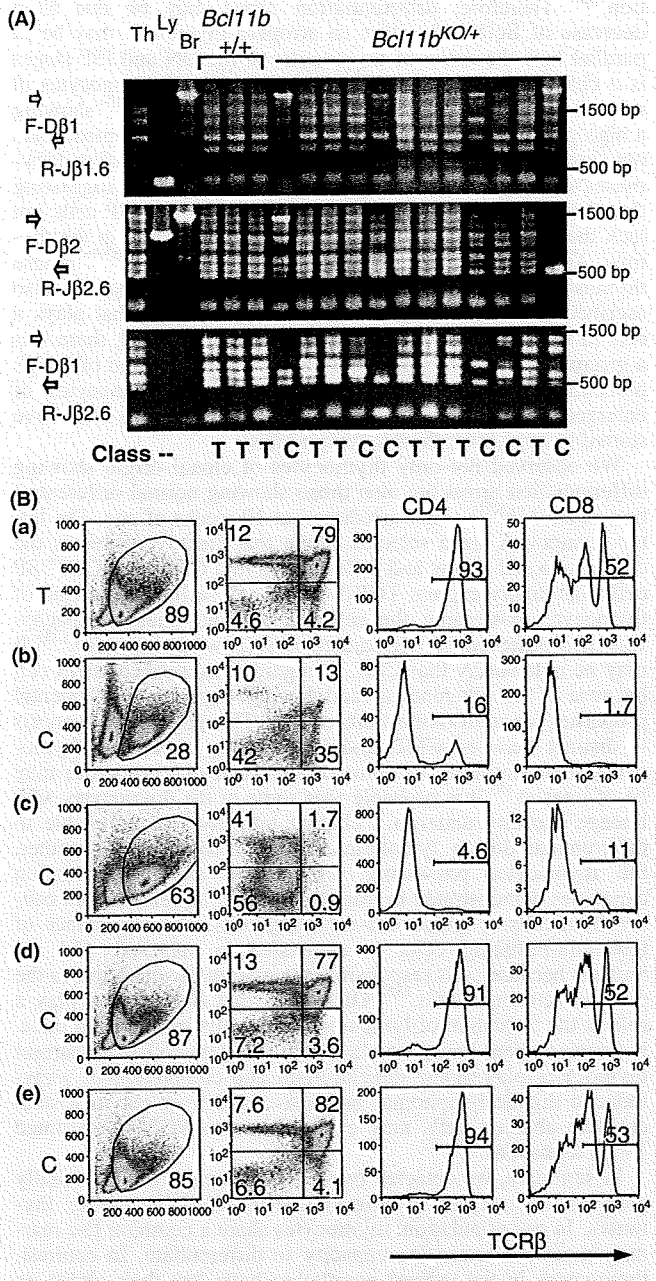

Fig. 5. Analyses of thymuses at 30 days after irradiation of *Bcl11b*$^{KO/+}$ mice at 10 weeks of age. (A) D-J rearrangement patterns at the *TCRβ* locus, as described in the legend for Figure 3(A). (B) Flow cytometry of CD4, CD8, and TCRβ expression in thymocytes, as described in the legend for Figure 4. T- or C-type thymus is shown at left.

DN percentages, indicative of some differentiation arrest before the DP cell stage, suggested the possibility of an abnormal increase in Wnt/β-catenin signaling.[21–23] Therefore, we examined the expression levels of β-catenin and interleukin-7 receptor (IL-7R), a cell surface receptor downstream from β-catenin signaling.[26,27] Figure 6(A) shows examples of flow cytometric analysis of *Bcl11b*$^{+/+}$ and *Bcl11b*$^{KO/+}$ thymocytes, as well as thymocytes from *Apc*$^{min/+}$ mice as a control. The Apc protein is a component of the degradation complex that modifies and regulates the β-catenin protein level.[23] Consistent with previous reports,[27,28] β-catenin was expressed at higher levels in DN

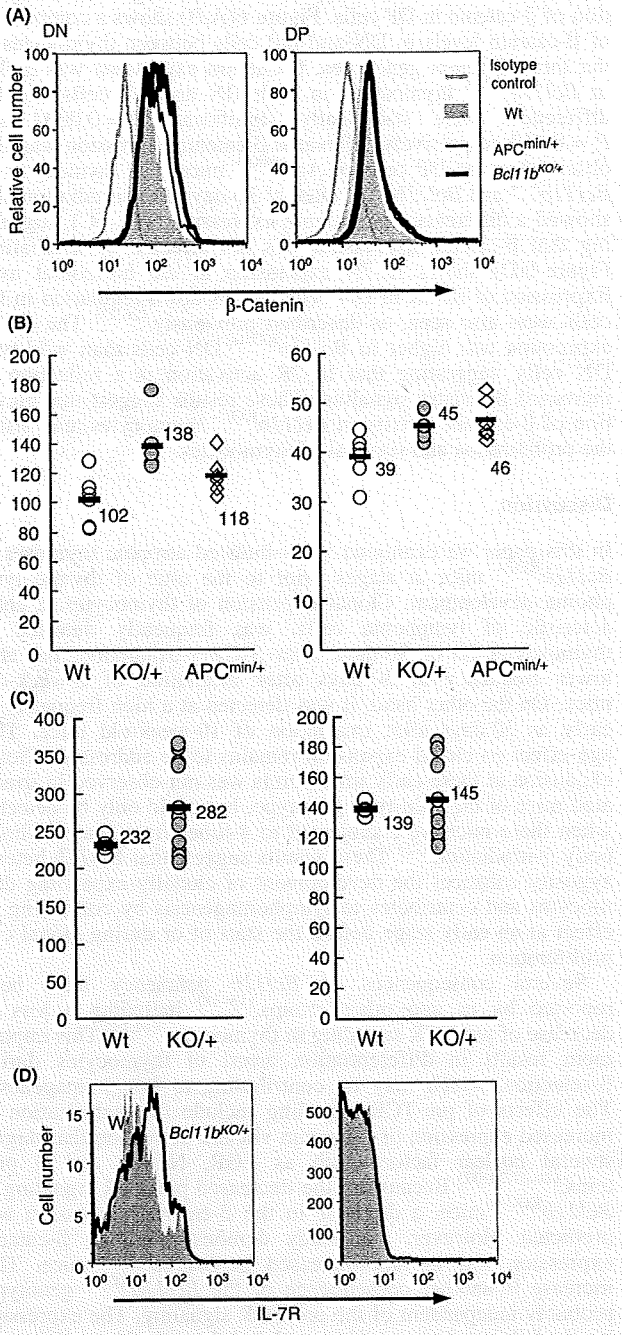

Fig. 6. Flow cytometry of β-catenin and interleukin-7 receptor (IL-7R) expression. (A) β-catenin expression in double-negative (DN) and double-postive (DP) cells of *Bcl11b*$^{+/+}$ (gray region), *Bcl11b*$^{KO/+}$ (bold black line), and *Apc*$^{min/+}$ (thin black line) mouse thymocytes. DN cells, left; DP cells, right. Isotype-matched staining control for *Bcl11b*$^{+/+}$ thymocytes is shown for comparison (gray line). The vertical axis shows relative cell number and the horizontal axis displays β-catenin expression. (B) The mean fluorescence intensity of β-catenin is compared between thymocytes of the three different genotypes. *P*-values in DN and DP cells between *Bcl11b*$^{+/+}$ and *Bcl11b*$^{KO/+}$ mice were 0.0034 and 0.019, respectively. The *P*-value in DP cells between wild-type and *Apc*$^{min/+}$ mice was 0.017. Comparison of the percent of β-catenin-positive cells showed similar results (not shown). (C) Mean fluorescence intensity of β-catenin in thymocytes compared between wild-type (gray circles) and *Bcl11b*$^{KO/+}$ (closed black circles) mice at 30 days after irradiation. (D) IL-7R expression in DN and DP cells of wild-type (gray region) and *Bcl11b*$^{KO/+}$ (black line) mouse thymocytes.

cells than DP cells in wild-type mice, indicating a down-regulation of β-catenin in DP cells. Figure 6(A,B) shows a comparison of β-catenin levels in DN and DP cells between thymocytes in the three different genotypes. β-Catenin expression was higher in *Bcl11b*$^{KO/+}$ thymocytes in both DN and DP cells and the differences were statistically significant ($P = 0.0034$ and $P = 0.019$, respectively). Elevated β-catenin expression was also observed in the DP cells of *Apc*$^{min/+}$ mice. DN thymocytes of *Bcl11b*$^{+/+}$ and *Bcl11b*$^{KO/+}$ mice at 30 days after irradiation also showed a difference in β-catenin expression (Fig. 6C), suggesting that β-catenin expression was not affected by irradiation. Figure 6(D) shows IL-7R expression at the horizontal axis. Expression of IL-7R in DN cells and its down-regulation in DP cells were also seen, as described previously.[26,27] The IL-7R expression was higher in *Bcl11b*$^{KO/+}$ DN cells than wild-type DN cells, suggesting that IL-7R activation is a reflection of increased β-catenin signaling. These results suggest that elevation of β-catenin activity in *Bcl11b*$^{KO/+}$ thymocytes may affect the proliferation and survival of thymocytes.

Discussion

In this paper we examined γ-ray-induced atrophic thymuses in *Bcl11b*$^{KO/+}$ mice at stages prior to the time of thymic lymphoma development. Clonal expansion of thymocytes, a characteristic of lymphoma cells, was frequently detected in thymuses at 60 or 80 days after 3-Gy γ-irradiation, but at a lower frequency at 30 days after irradiation of 8-week-old mice. On the other hand, it was detected at a high frequency as early as 30 days after irradiation of 10-week-old mice. This age effect on clonal expansion remains to be addressed. Clonal expansion at these early time points was not observed in irradiated mice of the wild-type genotype, but could only be detected when these mice were subjected to 4-times fractionated whole-body γ-irradiation.[25] These results suggest that *Bcl11b* heterozygosity enhances the development of clonally expanding thymocytes and contributes to lymphomagenesis by conferring an effect at an early stage before the start of or during clonal cell proliferation.

Several consequences of *Bcl11b* deficiency have been reported by us and other groups,[13–18] including a loss or decrease of pre-TCR signaling in thymocytes.[14,19] This impairment results in differentiation arrest of thymocytes during β-selection, which may be contributing to lymphomagenesis. The effects of pre-TCR signaling include the stabilization or increased expression of β-catenin via Erk activation that targets several nuclear factors such as EGR, NFAT, and E proteins.[26,27,29–32] Because of the decreased pre-TCR signaling in *Bcl11b*$^{KO/+}$ mice, a decrease in the β-catenin expression was predicted. However, this study demonstrated that β-catenin expression was in fact increased in *Bcl11b*$^{KO/+}$ mice. This increase is another consequence of the *Bcl11b*$^{KO/+}$ genotype, probably independent of the pre-TCR signaling. The expression level of β-catenin is mainly regulated through the modification by a degradation complex consisting of axin, Apc, GSK3β, and CKI.[23,33] Although the mechanism is not known, Bcl11b might affect the expression of some of those proteins. We infer that the increase of β-catenin plays a key role in lymphomagenesis, because β-catenin is a well-known oncogenic transcription factor and its stabilization predisposes thymocytes to malignant transformation.[34] β-Catenin targets promoters of *c-myc* and cyclin D1 in a complex with Tcf1 or Lef1, which positively regulate cell cycle progression.[23,33]

Differentiation arrest of thymocytes at the DN or ISP stages was observed in most thymuses that showed clonal expansion. This arrest was not seen in clonally expanded thymocytes induced in *Bcl11b* wild-type mice by fractionated γ-irradiation.[25] Therefore, differentiation arrest may be due to a decrease of Bcl11b function in atrophic thymus. It may be in parallel how the arrest of thymocytes at the DN and ISP stages is a characteristic of *Bcl11b*$^{KO/KO}$ mice.[13] ISP thymocytes in normal thymus are known to be highly proliferative,[35] showing a high percentage of S-phase cells (45% in our experiment; data not shown). However, the ISP cells observed in γ-irradiated thymuses showed low percentages (approximately 5%), suggesting that the thymocytes are phenotypically similar to ISP cells but lack the property of being able to highly proliferate in the thymus. Another finding observed in irradiated *Bcl11b*$^{KO/+}$ mouse thymuses was the decrease in cell number. This may be also ascribed to the decrease of the preTCR signaling that plays a role in survival of thymocytes.[13] On the other hand, there was a group of C-type thymuses with a low cellularity and of a high percentage of middle-sized G1 cells. Those thymocytes of enlarged cell-size might be the prelymphoma cells that have started to form overt thymic lymphomas.

We observed not only thymocytes of clonal origin showing differentiation arrest but also those showing normal differentiation in *Bcl11b*$^{KO/+}$ mice irradiated at 10 weeks of age. The latter thymocytes are a selected clone that already possesses the capacity to self-renew and differentiate into CD4$^+$ and CD8$^+$ SP cells that highly express TCRβ on the cell surface. This kind of thymocyte, possessing the self-renewal and lineage capacity, was also observed in γ-irradiated *Bcl11b* wild-type mice.[25] It may be noteworthy that CML is regarded as a cancer stem cell because of its self-renewal and lineage capacity, fundamental properties for adult tissue stem cells.[6] Though the pathogenesis is distinct between CML and the clonally expanding thymocytes, their similarity in terms of stem cell-like properties may be of interest.[6] It is probable that some of the thymocytes with lineage capacity undergo a change into thymocytes unable to differentiate during lymphoma development. Taken together, the thymocytes possessing self-renewal and differentiation capacities demonstrated in this paper might be related with cancer stem cells or lymphoma-initiating cells. The importance of leukemia-initiating cells is suggested in relapsed ALL in humans because cells responsible for relapse are ancestral to the primary leukemia cells.[36] Of note is that *Bcl11b* may play a role in the formation of lymphoma stem cells in irradiated mice. It remains open, however, what role the stem cell-like aberrant thymocytes play in the development and completion of γ-ray-induced thymic lymphomas and also whether or not such stem cell-like aberrant cells may exist in human *BCL11b*-disrupted T-cell leukemias.[10–12]

In summary, we detected two distinct populations of clonally growing thymocytes in γ-irradiated *Bcl11b*$^{KO/+}$ mouse thymuses. In one population, thymocytes share a common D-J rearrangement but retain the capacity to differentiate. In contrast, thymocytes in the second population have lost their ability to differentiate. Those thymocytes are not fully malignant because of the low cell number, and therefore, the establishment of thymic lymphomas requires an additional change for proliferation to reach completion. The *Bcl11b*$^{KO/+}$ genotype probably influences the clonal expansion and differentiation arrest of thymocytes in γ-irradiated mice and this may be ascribed in part to an increase in the level of β-catenin.

Acknowledgments

We thank Drs Minh To and Yuichi Wakabayashi for critical reading of this manuscript. This work was supported by Grants-in-Aid of Third Term Comprehensive Control Research for Cancer from the Ministry of Health, Labor and Welfare of Japan and for Cancer Research from the Ministry of Education, Science, Technology, Sports, and Culture of Japan.

doi: 10.1111/j.1349-7006.2010.01546.x

References

1 Hanahan D, Weinberg RA. The hallmarks of cancer. *Cell* 2000; **100**: 57–70.
2 Hahn WC, Weinberg RA. Modelling the molecular circuitry of cancer. *Nat Rev Cancer* 2002; **2**: 331–41.
3 Calabretta B, Perrotti D. The biology of CML blast crisis. *Blood* 2004; **103**: 4010–22.
4 Mullighan CG, Goorha S, Radtke I *et al.* Genome-wide analysis of genetic alterations in acute lymphoblastic leukaemia. *Nature* 2007; **446**: 758–64.
5 Mullighan CG, Miller CB, Radtke I *et al.* BCR-ABL1 lymphoblastic leukaemia is characterized by the deletion of Ikaros. *Nature* 2008; **453**: 110–4.
6 Clarke MF, Dick JE, Dirks PB *et al.* Cancer stem cells – perspectives on current status and future directions: AACR Workshop on cancer stem cells. *Cancer Res* 2006; **66**: 9339–44.
7 Wakabayashi Y, Inoue J, Takahashi Y *et al.* Homozygous deletions and point mutations of the Rit1/Bcl11b gene in γ-ray induced mouse thymic lymphomas. *Biochem Biophys Res Commun* 2003; **301**: 598–603.
8 Kominami R, Niwa O. Radiation carcinogenesis in mouse thymic lymphomas. *Cancer Sci* 2006; **97**: 575–81.
9 Kaminura K, Mishim O, Ohi H *et al.* Haploinsufficiency of Bcl11b for suppression of lymphomagenesis and thymocyte development. *Biochem Biophys Res Commun* 2007; **355**: 538–42.
10 Nagel S, Kaufmann M, Drexler HG, MacLeod RA. The cardiac homeobox gene NKX2-5 is deregulated by juxtaposition with BCL11B in pediatric T-ALL cell lines via a novel t(5;14)(q35.1;q32.2). *Cancer Res* 2003; **63**: 5329–34.
11 MacLeod RA, Nagel S, Kaufmann M, Janssen JW, Drexler HG. Activation of HOX11L2 by juxtaposition with 3'-BCL11B in an acute lymphoblastic leukemia cell line (HPB-ALL) with t(5;14)(q35;q32.2). *Genes Chromosomes Cancer* 2003; **37**: 84–91.
12 Przybylski GK, Dik WA, Wanzeck J *et al.* Disruption of the BCL11B gene through inv(14)(q11.2q32.31) results in the expression of BCL11B-TRDC fusion transcripts and is associated with the absence of wild-type BCL11B transcripts in T-ALL. *Leukemia* 2005; **19**: 201–8.
13 Wakabayashi Y, Watanabe H, Inoue J *et al.* Bcl11b is required for differentiation and survival of αβT lymphocytes. *Nat Immunol* 2003; **4**: 533–9.
14 Inoue J, Kanefuji T, Okazuka K, Watanabe H, Mishima Y, Kominami R. Expression of TCRβ partly rescues developmental arrest and apoptosis of αβT cells in Bcl11b-/- mice. *J Immunol* 2006; **176**: 5871–9.
15 Arlotta P, Molyneaux BJ, Chen J, Inoue J, Kominami R, Macklis JD. Neuronal subtype-specific genes that control corticospinal motor neuron development in vivo. *Neuron* 2005; **45**: 207–21.
16 Golonzhka O, Liang X, Messaddeq N *et al.* Dual role of COUP-TF-interacting protein 2 in epidermal homeostasis and permeability barrier formation. *J Invest Dermatol* 2008; **129**: 1459–70.
17 Golonzhka O, Metzger D, Bornert JM *et al.* Ctip2/Bcl11b controls ameloblast formation during mammalian odontogenesis. *Proc Natl Acad Sci USA* 2009; **106**: 4278–83.
18 Avurum Albu DI, Feng D, Bhattacharya D *et al.* BCL11B is required for positive selection and survival of double-positive thymocytes. *J Exp Med* 2007; **204**: 3003–15.
19 Okazuka K, Wakabayashi Y, Kashihara M *et al.* p53 prevents maturation of T cell development to the immature CD4-CD8+ stage in Bcl11b-/- mice. *Biochem Biophys Res Commun* 2005; **328**: 545–9.
20 Fischer A, Malissen B. Natural and engineered disorders of lymphocyte development. *Science* 1998; **280**: 237–43.
21 Gounari F, Aifantis I, Khazaie K *et al.* Somatic activation of beta-catenin bypasses pre-TCR signaling and TCR selection in thymocyte development. *Nat Immunol* 2001; **2**: 863–9.
22 Xu Y, Banerjee D, Huelsken J, Birchmeier W, Sen JM. Deletion of beta-catenin impairs T cell development.Nat Immunol. *Nat Immunol* 2003; **4**: 1177–82.
23 Staal FJ, Clevers HC. Wnt signaling in the thymus. *Curr Opin Immunol* 2003; **15**: 204–8.
24 Ohi H, Mishima Y, Kamimura K, Maruyama M, Sasai K, Kominami R. Multi-step lymphomagenesis deduced from DNA changes in thymic lymphomas and atrophic thymuses at various times after γ-irradiation. *Oncogene* 2007; **26**: 5280–9.
25 Yamamoto T, Morita S, Go R *et al.* Clonally expanding thymocytes having lineage capability in g-ray induced mouse strophic thymus. *Int J Radiat Oncol Biol Phys* (in press).
26 Xu M, Sharma A, Wiest DL, Sen JM. Pre-TCR-induced β-catenin facilitates transversal through β-selection. *J Immunol* 2009; **182**: 751–8.
27 Xu M, Sharma A, Hossain MZ, Wiest DL, Sen JM. Sustained expression of pre-TCR induced beta-catenin in post-beta-selection thymocytes blocks T cell development. *J Immunol* 2009; **182**: 759–65.
28 Weerkamp F, Baert MR, Naber BA *et al.* Wnt signaling in the thymus is regulated by differential expression of intracellular signaling molecules. *Proc Natl Acad Sci USA* 2006; **103**: 3322–6.
29 Carleton M, Haks MC, Smeele SA *et al.* Early growth response transcription factors are required for development of $CD4^-CD8^-$ thymocytes to the $CD4^+CD8^+$ stage. *J Immunol* 2002; **168**: 1649–58.
30 Xi H, Kersh GJ. Early growth response gene 3 regulates thymocyte proliferation during the transition from $CD4^-CD8^-$ to $CD4^+CD8^+$. *J Immunol* 2004; **172**: 964–71.
31 Aifantis I, Gounari F, Scorrano L, Borowski C, von Boehmer H. Constitutive pre-TCR signaling promotes differentiation through Ca^{2+} mobilization and activation of NF-kappaB and NFAT. *Nat Immunol* 2001; **2**: 403–9.
32 Engel I, Murre C. E2A proteins enforce a proliferation checkpoint in developing thymocytes. *EMBO J* 2004; **23**: 202–11.
33 Gregorieff A, Clevers H. Wnt signaling in the intestinal epithelium: from endoderm to cancer. *Genes Dev* 2005; **19**: 877–90.
34 Guo Z, Dose M, Kovalovsky D *et al.* Beta-catenin stabilization stalls the transition from double-positive to single-positive stage and predisposes thymocytes to malignant transformation. *Blood* 2007; **109**: 5463–72.
35 Ioannidis V, Beermann F, Clevers H, Held W. The β-catenin-TCF-1 pathway ensures $CD4^+CD8^+$ thymocyte survival. *Nat Immunol* 2001; **2**: 691–7.
36 Mullighan CG, Phillips LA, Su X *et al.* Genomic analysis of the clonal origins of relapsed acute lymphoblastic leukemia. *Science* 2008; **322**: 1377–80.

Adiponectin inhibits colorectal cancer cell growth through the AMPK/mTOR pathway

MICHIKO SUGIYAMA[1], HIROKAZU TAKAHASHI[1], KUNIHIRO HOSONO[1], HIROKI ENDO[1], SHINGO KATO[1], KYOKO YONEDA[1], YUICHI NOZAKI[1], KOJI FUJITA[1], MASATO YONEDA[1], KOICHIRO WADA[2], HITOSHI NAKAGAMA[3] and ATSUSHI NAKAJIMA[1]

[1]Division of Gastroenterology, Yokohama City University School of Medicine, 3-9 Fuku-ura, Kanazawa-ku, Yokohama; [2]Department of Pharmacology, Graduate School of Dentistry, Osaka University, 1-8 Yamadaoka, Suita, Osaka; [3]Biochemistry Division, National Cancer Center Research Institute, 1-1 Tsukiji 5-chome, Chuo-ku, Tokyo, Japan

Received July 2, 2008; Accepted September 25, 2008

DOI: 10.3892/ijo_00000156

Abstract. Adiponectin is a peptide hormone secreted by adipose tissue. It is a key hormone responsible for insulin sensitization, and its circulating level is inversely associated with abdominal obesity. Recent studies have shown that a reduced plasma adiponectin level is significantly correlated with the risk of various cancers. However, there are few studies regarding the association of adiponectin and colorectal cancer. To address this issue, we investigated the effect of adiponectin on colorectal cancer cells. Three colorectal cancer cell lines express both AdipoR1 and AdipoR2 receptors. MTT assay revealed that adiponectin inhibited human colorectal cancer cell growth. Furthermore, Western blot analysis revealed that adiponectin activated adenosine monophosphate-activated protein kinase (AMPK) and suppressed mammalian target of rapamycin (mTOR) pathways. Selective AMPK inhibitor compound C abrogated the inhibitory effect of adiponectin on cell growth. Our results clearly demonstrate the novel findings that adiponectin inhibits colorectal cancer cell growth via activation of AMPK, thereby down-regulating the mTOR pathway.

Introduction

Colorectal cancer (CRC) is one of the most common malignancies. Obesity, especially visceral obesity, has been reported to be associated with CRC (1,2). Adipose tissue is not only a fat storage organ, but it secretes several bioactive substances known as adipocytokines (3,4). Adiponectin is secreted from adipocytes and is a key hormone responsible for insulin sensitization (5-12). Its plasma level is dramatically decreased in patients with obesity and type 2 diabetes mellitus (DM) (4,5,13). Since both obesity and type 2 DM have been reported to be associated with an elevated risk of CRC (14), it is speculated that the plasma level of adiponectin may be related to the risk of CRC. However, several contradictory results have been reported from human clinical studies on the relationship between the plasma levels of adiponectin and the risk of CRC (15,16).

It is well known that the adiponectin receptor exists in two isoforms: adiponectin receptor 1 (AdipoR1) and 2 (AdipoR2) (17). These receptors mediate cellular functions by activating intracellular signaling pathways (17). The molecular pathways downstream of AdipoRs remain to be fully elucidated, but studies in metabolically-responsive cells have shown that activation of the pleiotropic adenosine monophosphate-activated protein kinase (AMPK) is involved in the signaling cascade downstream of adiponectin receptors (18,19). AMPK plays a key role in the regulation of energy homeostasis and acts as a 'metabolic sensor' to regulate adenosine triphosphate (ATP) concentrations (20). It is also associated with cell growth; phosphorylated AMPK suppresses mammalian target of rapamycin (mTOR) signaling pathway (21,22). mTOR plays a central role in the regulation of cell proliferation, growth, differentiation, migration and survival (23-26), and may be abnormally regulated in tumors (23,27-29). The 70-kDa ribosomal protein S6 kinase (p70S6K) and S6 ribosomal protein (S6P) are part of the signaling cascade downstream of mTOR; they are activated via phosphorylation by mTOR (28,30,31). Non-cleaved adiponectin (full-length adiponectin; f-adiponectin) and proteolytically-cleaved adiponectin containing a C-terminal globular region (globular adiponectin; g-adiponectin) were reported to have different affinities to AdipoR1 and AdipoR2 (17). In this study, we only examined the g-adiponectin because this isoform binds both receptors, while f-adiponectin has low affinity to AdipoR1 (17), and it exerts more potent effect than f-adiponectin (5). However, the expression levels of AdipoR1 and AdipoR2, the affinity of the different forms of

Correspondence to: Dr Atsushi Nakajima, Division of Gastroenterology, Yokohama City University School of Medicine, 3-9 Fuku-ura, Kanazawa-ku, Yokohama, Japan
E-mail: nakajima-tky@umin.ac.jp

Key words: adiponectin, colorectal cancer, cell growth, AdipoR1/AdipoR2, adenosine monophosphate-activated protein kinase